Provenance of Cenozoic sedimentary rocks from the Sulaiman fold and thrust belt, Pakistan: implications for the palaeogeography of the Indus drainage system

Martin Roddaz, Aymen Said, Stéphane Guillot, et al.

Journal of the Geological Society 2011; v. 168; p. 499-516
doi: 10.1144/0016-76492010-100

Journal of the Geological Society, London, Vol. **168**, 2011, pp. 499–516. doi: 10.1144/0016-76492010-100.

Provenance of Cenozoic sedimentary rocks from the Sulaiman fold and thrust belt, Pakistan: implications for the palaeogeography of the Indus drainage system

MARTIN RODDAZ[1]*, AYMEN SAID[1], STÉPHANE GUILLOT[2], PIERRE-OLIVIER ANTOINE[1], JEAN-MARC MONTEL[3], FRANÇOIS MARTIN[1] & JOSÉ DARROZES[1]

[1]*Université de Toulouse, UPS (SVT-OMP), IRD, CNRS, LMTG, 14 Av. Edouard Belin, F-31400 Toulouse, France*

[2]*IsTerre, CNRS, Université Grenoble I, BP 53, 38041 Grenoble cedex, France*

[3]*UMR 7655 G2R, Henri Poincaré University, Faculty of Sciences, BP 236, 54501 Vandoeuvre les Nancy, France*

**Corresponding author (e-mail: mroddaz@lmtg.obs-mip.fr)*

Abstract: The provenance of middle Eocene to early Miocene sedimentary rocks cropping out in the Sulaiman fold and thrust belt has been determined examining the mineralogy, bulk-rock major and trace elements, and Nd–Sr isotopes. The older (50–30 Ma) deposits are characterized by a mixed orogenic provenance with a major contribution from the Karakorum and the Tethyan belt (*c.* 80%). As the 50–30 Ma deposits have a provenance distinct from that of coeval Subathu, Khojak and Ghazij shallow marine formations of India and Pakistan, we propose that they were deposited as a distinct delta system that once fed the Palaeo-Indus fan. We document a major change in provenance that occurred before the early–late Oligocene transition at *c.* 30 Ma. This change in provenance is marked by the appearance of chlorite and monazite and a shift toward more radiogenic Nd–Sr isotopic compositions. We interpret this change as the result of the exhumation and erosion of the proto-Higher Himalaya. The 30–15 Ma sampled rocks are characterized by a major contribution from the Tethyan belt and the Higher Himalayan Crystallines (70–90%) and a subordinate contribution (10–30%) from the Karakorum, Ophiolitic Suture and Trans-Himalaya. As the εNd(0) values of our 30–15 Ma samples are similar to those of the Palaeo-Indus fan deposits, we suggest that the 30–15 Ma sedimentary rocks of the Sulaiman fold and thrust belt were the fluvial onshore record of the Indus fan. Other coeval deposits of India and Pakistan recorded similar increasing exhumation of the Higher Himalaya range, so that we postulate that these sedimentary rocks all derived from the Palaeo-Indus drainage basin. This would suggest that the modern Indus drainage basin is no younger than 30 Ma.

The Himalaya is the greatest mountain belt in the world and is by far the most important source of sediment input to the oceans (Summerfield & Hulton 1994; Hay 1998). Its denudation history is thus particularly important for understanding interactions between tectonics, erosion, and climate (Raymo & Ruddiman 1992; France-Lanord & Derry 1997). The early Himalayan highlands were formed by the early Palaeocene and have been shedding sediments ever since (Beck *et al.* 1995; Garzanti *et al.* 1996; Qayyum *et al.* 2001).

Many studies have used Neogene deposits to constrain the erosion and exhumation histories of the Himalaya (e.g. Burbank 1992; Burbank *et al.* 1993; Robinson *et al.* 2001; DeCelles *et al.* 2004; Clift & Blusztajn 2005; Bernet *et al.* 2006; Najman 2006; van der Beek *et al.* 2006). However, few studies have been devoted to Palaeogene foreland deposits (Najman 2006; Wu *et al.* 2007; Najman *et al.* 2008; Carter *et al.* 2010) because Oligocene deposits were thought not to be present in the Himalayan foothills (Welcomme & Ginsburg 1997; Welcomme *et al.* 2001). The Eocene to early Miocene period is when the Himalaya underwent significant crustal thickening, transition from shallow marine to continental deposits, exhumation of the Higher Himalaya, and initiation of the Indus drainage system (DeCelles *et al.* 1998; Clift *et al.* 2001*a*,*b*; Robinson *et al.* 2001; Sinclair & Jaffey 2001; Najman 2006).

Recent biostratigraphic studies of sedimentary rocks within the Sulaiman fold and thrust belt of Pakistan revealed the presence of shallow marine Eocene deposits, deltaic early Oligocene deposits and continental late Oligocene to early Miocene deposits (De Franceschi *et al.* 2008; Métais *et al.* 2009) that provide a unique opportunity to add to understanding of early orogenic growth. Based on clay mineralogy, Nd–Sr isotopic compositions and heavy mineral assemblages, the present study is aimed at determining the provenance and erosional history of the western Himalaya and nature of the Indus drainage basin during this period.

Geological background and sampling

Sediments that were eroded from the early western Himalayan orogenic highlands during Eocene to early Miocene times were deposited in the Indo-Pakistani western Himalayan foreland basin (Bossart & Ottiger 1989; Burbank *et al.* 1996; Pivnik & Wells 1996; Najman *et al.* 1997), in the Sulaiman fold and thrust belt (Waheed & Wells 1990; Jadoon *et al.* 1994*a*; Métais *et al.* 2009), in the Katawaz remnant ocean to form a delta–submarine-fan complex (Qayyum *et al.* 1996) and in the deep marine Indus fan (Clift *et al.* 2001*b*) (Figs 1 and 2). We sampled 17 sandstones and 16 mudstones from early Eocene to early Miocene deposits of the Bugti hills in the Sulaiman fold and thrust belt (Fig. 2).

Tectonic setting of the Sulaiman fold and thrust belt

The Sulaiman fold and thrust belt (see Fig. 1 for location) is the broadest fold and thrust belt of the Himalayan foreland basins (Jadoon *et al.* 1994*a*). It comprises a passive roof duplex (Banks & Warburton 1986) formed in response to the oblique collision

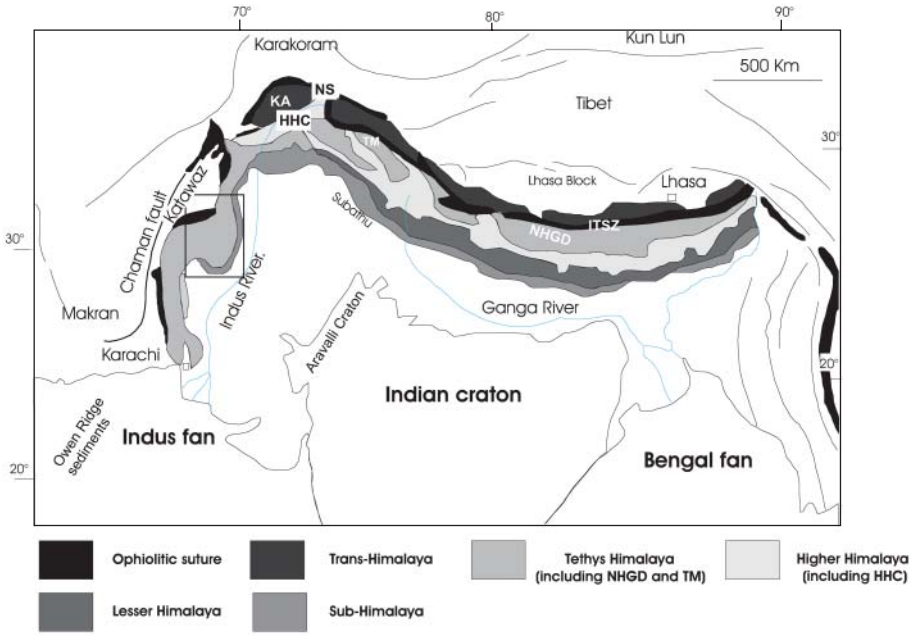

Fig. 1. Simplified geological map of Himalaya (modified from Najman 2006). Rectangle indicates the location of Figure 2. HHC, Higher Himalayan Crystallines; KA, Kohistan Arc; NHGD, North Himalayan gneissic domes; NS, Northern Suture; ITSZ, Indus–Tsangpo Suture Zone; TM, Tso Morari. (See Table 6 for main characteristics of these units.)

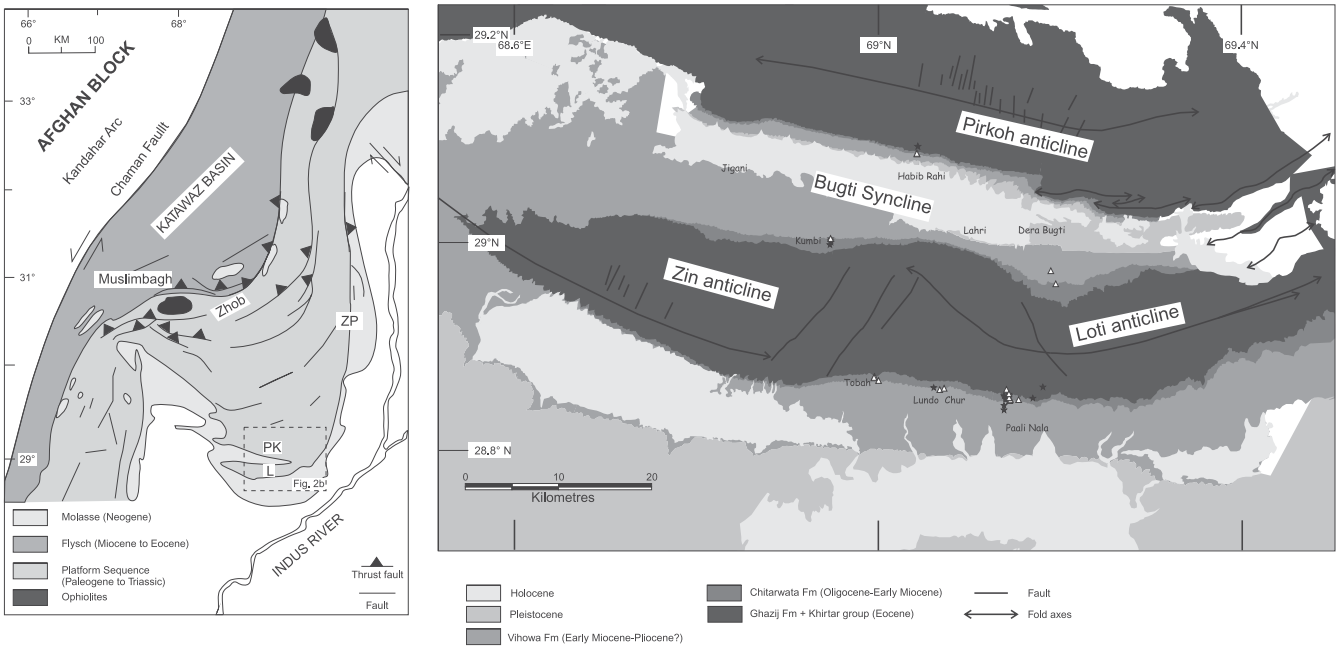

Fig. 2. (**a**) Generalized geological map of the Sulaiman fold and thrust belt (modified from Jadoon *et al.* 1994*a*). Box shows the location of (**b**). PK, Pirkoh anticline; L, Loti anticline; ZP, Zinda Pir dome. (**b**) Geological map of the study area. Location of sample outcrops is indicated by black stars (mudstones) and white triangles (sandstones). (See Table 1 for coordinates.)

between the Indian subcontinent and the Eurasia plate (Jadoon & Khurshid 1996). The initial collision event in the Sulaiman fold and thrust belt is recorded by the emplacement of the Muslimbagh ophiolites, which occurred either at the Cretaceous–Tertiary boundary (Gnos *et al.* 1997), or later in the Palaeocene–early Eocene (Allemann 1979). Since the late Oligocene–early Miocene, renewed southward thrusting has reworked the Palaeogene deposits as the deformation front migrated southward and eastward (Banks & Warburton 1986; Waheed & Wells 1990). The initiation of the Chaman left-lateral strike-slip fault occurred between the late Oligocene and the early Miocene, when the shortening to the south of the Muslimbagh ophiolites became significant (25 ± 5 Ma, Jadoon & Khurshid 1996). Southward thrusting of the Neogene deposits is still continuing (Jadoon *et al.* 1994*b*).

The frontal portion of the Sulaiman fold and thrust belt, which encompasses 10 000 km^2 of the Sulaiman Lobe, consists of an east–west-trending doubly plunging fold (Jadoon *et al.* 1994*b*).

Sequential restoration of a balanced cross-section across the Sulaiman fold and thrust belt shows that the Loti anticline (see Fig. 2 for location) first developed as a result of a broad concentric detachment folding at the fault tip (Jadoon *et al.* 1994*a*). This detachment was followed by the development of a passive roof duplex. Southward propagation of the duplex produced the Pirkoh anticline and the Bugti syncline (Jadoon *et al.* 1994*a*).

Stratigraphy of the Sulaiman fold and thrust belt and sampling strategy

The sedimentary succession of the Sulaiman fold and thrust belt (Fig. 3) includes: (1) the early Eocene Ghazij Formation; (2) the middle–late Eocene Kirthar group; (3) the Oligocene–early Miocene Chitarwata Formation; (4) the late early to middle Miocene Vihowa Formation; (5) the middle Miocene–Pliocene deposits of the Siwalik group.

The early Eocene Ghazij Formation records the first evidence of the collision between India and Eurasia (Warwick *et al.* 1998; Najman 2006). It consists of marine mudstones that pass upward to paralic sandstones and mudstones and to continental mudstones and conglomerates (Warwick *et al.* 1998) mainly derived from reworking of sedimentary rocks plus a subordinate igneous source that shed chromites and fragments of basic volcanic rocks, which may be indicative of an ophiolitic source (Warwick *et al.* 1998; Najman 2006). The middle–late Eocene Kirthar group consists of carbonates, marls and mudstone shelf deposits (Blanford, 1879; Williams 1959; Shah 1977; Gingerich *et al.* 1979). The Oligocene–early Miocene Chitarwata Formation consists of deltaic deposits at its base that grade upward to fluvial deposits (Métais *et al.* 2009). The Chitarwata Formation is widely exposed throughout the eastern part of the Sulaiman Range, and consists of coastal, deltaic, and fluvial deposits that have yielded numerous fossil vertebrates ranging from the earliest Oligocene to the late early Miocene (Antoine *et al.* 2010). At Chitarwata Post in the Zinda Pir dome (see location in Fig. 2a), the thickness of the Chitarwata Formation is *c*. 567 m (Lindsay *et al.* 2005) whereas in our study area, it does not exceed 260 m (Fig. 4). In the Zinda Pir area, the Chitarwata Formation was originally considered as entirely early Miocene in age on the basis of vertebrate fossil assemblages (Downing *et al.* 1993) and preliminary magnetostratigraphical data (Friedman *et al.* 1992). However, Lindsay *et al.* (2005) reinterpreted the magnetostratigraphical sequence of the Zinda Pir area in the light of new biostratigraphical data of Welcomme *et al.* (2001) and assigned an Oligocene–Early Miocene age to the Chitarwata Formation. The base of the fossiliferous sequence of the Chitarwata Formation in the Bugti Hills (0 and C2 horizons, Fig. 4) is early Oligocene in age as indicated by the foraminiferan and mammal biostratigraphy (Welcomme *et al.* 2001; Métais *et al.* 2009). As emphasized by these later researchers, the apparent discrepancy in age between deposits of the Zinda Pir area and those of the Bugti Hills could be due to the existence of many stratigraphic hiatuses. These hiatuses render the correlation between these two areas difficult to establish and explain the fact that the lower Member of the Chitarwata Formation ('Bugti Member') is a condensed sequence that may represent a time interval not yet recorded elsewhere in the Sulaiman fold and thrust belt (Fig. 4). The basal contact of the Chitarwata Formation with the Kirthar group is unconformable (Welcomme *et al.* 2001). The early to middle Miocene Vihowa Formation, made up of fluvial sandstones and microconglomerates associated with lacustrine marls, conformably overlies the Chitarwata Formation

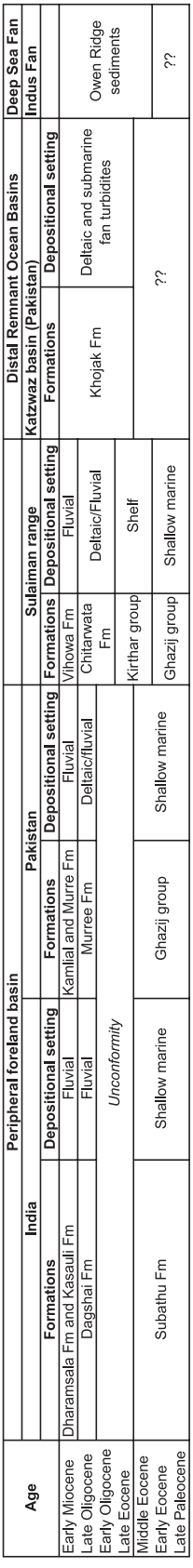

Fig. 3. Stratigraphical chart and depositional setting of western Himalayan sediment repositories (adapted from Najman 2006). Fm, Formation; Mb, Member.

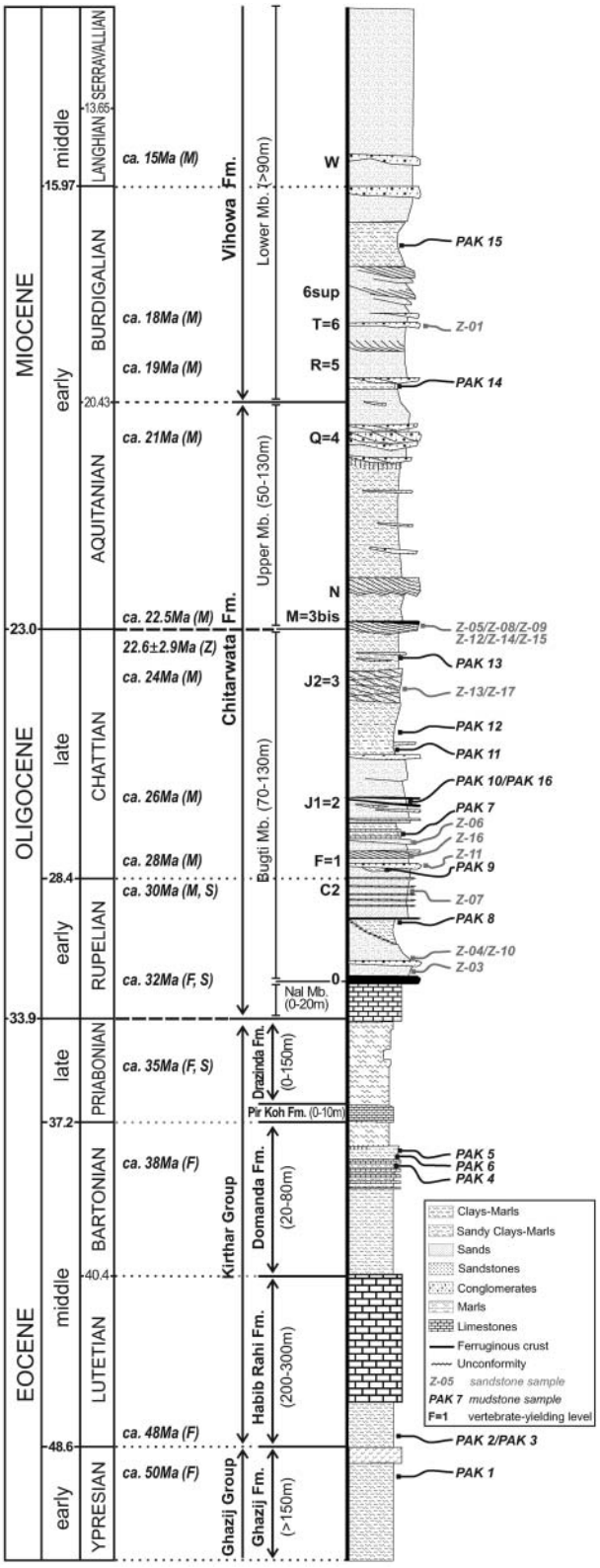

Fig. 4. Composite stratigraphic section of Cenozoic deposits of the study area and the location of mudstones (PAK1 to PAK16) and sandstones (Z-01 to Z-17) within the series. To the left, standard ages are those provided by Gradstein & Ogg (2006). In the middle column, the numeric ages provided are tentative and based on biochronology (M, mammals; S, selachians; F, foraminiferans). Modified from Welcomme *et al.* (2001), Antoine *et al.* (2003, 2004, 2010), Adnet *et al.* (2007) and Métais *et al.* (2009).

(Métais *et al.* 2009). Overlying the Vihowa Formation are fluvial deposits of the Siwalik group (Welcomme *et al.* 2001). Palaeocurrent measurements from planar cross-bedded and trough cross-bedded sandstones of the Chitarwata and Vihowa formations support a dominant southeastward palaeoflow direction during the deposition of these formations (Downing & Lindsay 2005). Waheed & Wells (1990) found a similar southward direction in the formation they called the post-Oligocene molasse of the Sulaiman Range, which is time equivalent of the Chitarwata and Vihowa formations.

To study further the provenance of these rocks, 17 sandstones (Z-01 to Z-17) and 16 mudstones (PAK 1 to PAK 16) from the Ghazij Formation, Kirthar group and Chitarwata and Vihowa formations were collected in 2004. Sample locations are shown in Table 1 and Figure 2. Figure 4 locates the samples in a composite stratigraphical column of the area (Fig. 4). The age of the samples ranges from early Eocene (*c.* 50 Ma) to early Miocene (18–15 Ma, Fig. 4).

Previous results on the provenance of coeval Eocene to early Miocene sedimentary rocks

Foreland basin of India. The foreland basin of India contains late Palaeocene–middle Eocene marine deposits of the Subathu Formation, and Oligocene–Miocene alluvial deposits of the Dagshai, Kasauli and Dharamsala formations (Fig. 3). The contact between the Subathu and Dagshai formations remains disputed. According to Najman *et al.* (2004), the contact is sharp and the base of the Dagshai Formation is characterized by a fluvial quartz-rich White Sandstone unit. Recent studies interpreted this White Sandstone unit as forced regressive shoreface deposits and proposed that this unit marked the top of the Subathu Formation (Bera *et al.* 2008, 2010) with a contact between the Subathu and Dagshai formations marked by an unconformity that constitutes the top of the White Sandstone unit.

Petrographic data indicate a predominant sedimentary provenance for the Subathu Formation with subordinate felsitic and rare serpentinite schist. Heavy mineral analyses show the predominance of spinel derived from an ophiolitic or arc source, which is in agreement with high Ni and Cr contents in the Subathu mudstones (Najman & Garzanti 2000). εNd(0) values of the Subathu Formation range from −7.8 to −10.8 with $^{87}Sr/^{86}Sr$ ratio varying between 0.708 and 0.717 (Najman *et al.* 2000; Bera *et al.* 2010). These Nd–Sr isotopes suggest a mixed northern provenance with contributions from the Tethys Himalaya and the Indus–Tsangpo Suture Zone (Najman *et al.* 2000). The White Sandstone unit and the deposits of the Daghsai Formation recorded a major change in provenance. Lithic fragments of very low-grade to low-grade metamorphic material are dominant (Najman & Garzanti 2000; White *et al.* 2002). εNd(0) values are more negative (−12.7 to −25.4) and $^{87}Sr/^{86}Sr$ ratio are more radiogenic (0.722–0.773) than those of the deposits of the Subathu Formation (Najman *et al.* 2000; Bera *et al.* 2010). Compared with the underlying Subathu Formation, mafic input decreases as attested by decreasing Ni and Cr content, very rare occurrences of spinel (Najman & Garzanti 2000), and a change in Nd–Sr isotopic compositions. Associated with occurrences of zircon and 'Himalayan-aged' micas, and the presence of lithic fragments of very low-grade to low-grade metamorphic material, these Nd–Sr isotopic compositions suggest that the White Sandstone unit and the Dagshai deposits were derived from the upper crustal levels of Higher Himalaya (Najman 2006). This dramatic change in provenance, with the elimination of the igneous source

Table 1. *Location, age and average grain size (mud or sand) for analysed sediments*

Sample	Locality	Formation	Age	Type	Latitude (°N)	Longitude (°E)
PAK 15	Paali	Vihowa	Early Miocene	Mudstone	28.83915	69.13851
PAK 14	Paali	Vihowa	Early Miocene	Mudstone	28.84345	69.13842
PAK 13	Kumbi	Chitarwata	Late Oligocene	Palaeosol	29.00396	68.94769
PAK 12	Kumbi	Chitarwata	Late Oligocene	Palaeosol	29.00202	68.94771
PAK 11	Kumbi	Chitarwata	Late Oligocene	Mudstone	29.00053	68.94819
PAK 10	Kumbi	Chitarwata	Late Oligocene	Mudstone	28.99828	68.94692
PAK 7	Paali	Chitarwata	Late Oligocene	Mudstone	28.8496	69.14032
PAK 16	Lundo	Chitarwata	Late Oligocene	Mudstone	28.86073	69.06124
PAK 9	Paali	Chitarwata	Late Oligocene	Mudstone	28.8508	69.14271
PAK 8	Paali	Chitarwata	Early Oligocene	Mudstone	28.85213	69.14321
PAK 5	Beamshai	Khirtar	Middle Eocene	Mudstone	28.85278	69.13841
PAK 6	Paali	Khirtar	Middle Eocene	Mudstone	28.85428	69.14397
PAK 4	Sajji	Khirtar	Middle Eocene	Mudstone	28.85048	69.17015
PAK 3	Sajji nord	Khirtar	Middle Eocene	Mudstone	28.86119	69.1812
PAK 2	Habib Rahi	Khirtar	Middle Eocene	Mudstone	29.09291	69.0436
PAK 1	Habib Rahi	Ghazij	Early Eocene	Mudstone	29.09291	69.0436
Z-01	Harga	Vihowa	Early Miocene	Sand	28.97289	69.18997
Z-05	Paali	Chitarwata	Early Miocene	Sand	28.84785	69.14476
Z-08	Kumbi	Chitarwata	Early Miocene	Sand	29.00396	68.94769
Z-09	Harga	Chitarwata	Early Miocene	Sand	28.96028	69.19535
Z-12	Habib Rahi	Chitarwata	Early Miocene	Sand	29.08519	69.04289
Z-14	Lundo	Chitarwata	Early Miocene	Sand	28.85844	69.06775
Z-15	Tobah	Chitarwata	Early Miocene	Sand	28.86719	69.00054
Z-02	Paali	Chitarwata	Late Oligocene	Sand	28.84785	69.14476
Z-17	Habib Rahi	Chitarwata	Late Oligocene	Sand	29.08581	69.04258
Z-13	Lundo	Chitarwata	Late Oligocene	Sand	28.85977	69.07256
Z-11	Tobah	Chitarwata	Late Oligocene	Sand	28.87113	68.99616
Z-06	Paali	Chitarwata	Late Oligocene	Sand	28.84891	69.14551
Z-16	Pazbogi	Chitarwata	Late Oligocene	Sand	28.84881	69.15456
Z-07	Paali	Chitarwata	Early Oligocene	Sand	28.85059	69.14419
Z-04	Beamshai	Chitarwata	Early Oligocene	Sand	28.85861	69.14113
Z-10	Tobah	Chitarwata	Early Oligocene	Sand	28.87016	68.99554
Z-03	Paali	Chitarwata	Early Oligocene	Sand	28.85452	69.14393

and the appearance of a metamorphic source, is interpreted to result from the suddenly accelerated surface uplift of the Tso Morari North Himalayan gneissic unit and Zanskar Higher Himalayan Crystallines by Oligocene times (Bera *et al.* 2010). Nd–Sr isotopic compositions of the overlying Kasauli Formation are similar to that of the Dagshai Formation, but petrography and heavy mineral data indicate erosion of the deeper level of the Higher Himalayan Crystallines with the appearance of garnet of almandine type (Najman & Garzanti 2000). Nd–Sr isotopic compositions and Ar–Ar age of detrital mineral as well as petrographical and heavy mineral data document rapid erosion of the Higher Himalayan Crystallines during the deposition of the Lower Dharamsala Member (20–17 Ma) (White *et al.* 2002). The deposition of the Upper Dharamsala Member (17–13 Ma) is accompanied by an abrupt change in the petrographical characteristics and mica age populations. A major influx of micas having pre-Himalayan ages, and input of sedimentary and very low- to low-grade metamorphic lithic fragments documented an additional source interpreted as an unmetamorphosed or low-grade Higher Himalayan protolith (White *et al.* 2002).

Foreland basin of Pakistan (excluding Sulaiman fold and thrust belt). The peripheral foreland basin of Pakistan is filled with Palaeocene–Eocene marine deposits known under various local names (including the Ghazij group) unconformably overlain by Oligocene–Miocene deltaic to continental deposits of the Murree Formation and by deposits of the Kamlial Formation (Fig. 3) that were magnetostratigraphically dated at 18–14 Ma (Johnson *et al.* 1985). The Balakot Formation is considered to be part of the Murree Formation (Najman 2006).

Detrital modes indicate a predominant sedimentary source with some metamorphic input for early to middle Eocene marine deposits of the Ghazij group (Pivnik & Wells 1996). Oligocene–Miocene red beds of the Murree Formation contain both low-grade metasedimentary to sedimentary detritus derived from proto-Himalayan thrust sheets and volcanic to ophiolitic detritus derived both from the arc and suture zone (Critelli & Garzanti 1994). Chromite composition is similar to that found in the Indian foreland Subathu Formation (Najman & Garzanti 2000). This major change from a sedimentary source for Eocene marine deposits to a metamorphic sources for the Oligocene–Miocene is interpreted to document the first major input from the rising Himalaya thrust belt (Najman 2006). The sedimentary rocks of the Kamlial Formation are characterized by a dominant magmatic arc provenance and 'subordinate contribution from a rapidly exhuming source' (Najman *et al.* 2003).

Katawaz remnant ocean basin. The deposits of the Katawaz basin consist of late Eocene to early Miocene deltaic and submarine fan turbidites of the Khojak Formation (Qayyum *et al.* 1996, 2001; Fig. 3). They were interpreted to represent the Palaeogene Indus delta–fan complex (Qayyum *et al.* 1997). Lithic fragments are dominated by sedimentary clasts, followed by subordinate low-grade metamorphic clasts and rare volcanic lithic fragments (Qayyum *et al.* 2001). The proportion of low-grade metamorphic clasts rises during the Oligocene (Qayyum *et al.* 2001). Accessory minerals include titanite, zircon, magnetite, hornblende, olivine pyroxene, epidote, glauconite and pyrite, as described by Qayyum *et al.* (2001). According to those researchers, the predominance of sedimentary and low-grade meta-

morphic clasts suggests early derivation from a collision orogen, and the scarcity of volcanic lithic fragments dismisses the magmatic arc as a main source. A recent multidisciplinary provenance study involving sediment petrography, U–Pb and fission-track dating of detrital zircon suggested a similar provenance for Palaeogene deposits of the Katawaz basin and of the Makran region of southern Iran, consistent with a source in the nascent western Himalaya and associated magmatic arc (Carter *et al.* 2010).

Indus fan. Significant pre-Miocene deposits have been identified from offshore seismic data and drilling on the Owen Ridge in the Oman Sea (Deep Sea Drilling Project (DSDP) Site 224). Based on subsurface data, Clift *et al.* (2001*b*) estimated that 35% of the Indus fan sediments predate the early Miocene uplift of the Murray Ridge (*c*. 22 Ma). Minerals present in the sediment include hornblende, pyroxene, monazite, garnet, sillimanite, kyanite and muscovite (Kidd & Davies 1978; Najman 2006). εNd(0) values of middle Eocene to middle Oligocene Indus fan deposits range from −10.9 to −13.07 (mean *c*. −11.9) with the exception of one anomalous sample having εNd(0) of −5.52 (Clift *et al.* 2001*b*). Late Oligocene to early Miocene Indus fan deposits have similar εNd(0) values to those of middle Oligocene to middle Eocene (−11.10 to −12.43; mean *c*. −11.5; Clift *et al.* 2001*b*). Unradiogenic detrital K-feldspar Pb isotopic compositions and εNd(0) values less negative than those in the Higher Himalaya suggest contributions from igneous rocks in, or north of, the suture zone (Clift *et al.* 2001*b*). However, a strictly Himalayan source is disputed because no evidence of Palaeogene material of sufficient metamorphic grade has been found inland (Najman 2006).

Analytical methods

Each heavy mineral was obtained via a standard separation of 2 kg samples, first in the field using a sand pan, then in the laboratory following standard heavy mineral separation techniques. Heavy minerals were then inspected under an optical microscope and grouped into species that have the same optical properties. The minerals were identified by means of scanning electronic microscopy (SEM) at the Laboratoire des Mécanismes et Transferts en Géologie (University of Toulouse).

The mineralogical composition of the 16 mudstones was determined by X-ray diffraction (XRD) using a Philips PW1050 diffractometer (INGEIS) with Cu K radiation operated at 40 mA and 30 kV. The 16 mudstones were then analysed for major and trace element concentrations and Nd–Sr isotopic compositions. Major elements were measured by inductively coupled plasma atomic emission spectrometry (ICP-AES) (Thermo-Electron, Iris Intrepid II). The international geostandard SRM 1646a estuarine sediment was used to check the efficiency of both the acid digestion protocol and the analysis. Our measurements are in good agreement (close to 5%) with the recommended values.

Trace element concentrations were measured by inductively coupled plasma mass spectrometry (ICP-MS) (Perkin Elmer, Elan 6000) and Nd–Sr isotopic ratios were measured by thermal ionization mass spectrometry (TIMS) using a Finnigan Mat 261 system in dynamic mode following Roddaz *et al.* (2005, 2006). The measured $^{143}Nd/^{144}Nd$ ratios are presented as the fractional deviation in parts per 10^4 (units) from $^{143}Nd/^{144}Nd$ in a Chondritic Uniform Reservoir (CHUR) as measured at the present day: $\varepsilon_{Nd}(0) = [(^{143}Nd/^{144}Nd)_S/I_{CHUR}(0) - 1] \times 10^4$, where $(^{143}Nd/^{144}Nd)_S$ is the present-day ratio measured in the sample and $I_{CHUR}(0)$ is the $^{143}Nd/^{144}Nd$ in the CHUR reference reservoir at the present ($I_{CHUR}(0) = 0.512638$; (Jacobsen & Wasserburg 1980).

Results

Mineralogy

Clay mineralogy of mudstones. The results are reported in Table 2. The lacustrine marl samples PAK 4, PAK 5 and PAK 6 (middle Eocene) consist of calcite and kaolinite and do not contain quartz. Post-Eocene samples are characterized by the occurrence of quartz and smectite. The late Oligocene–early Miocene samples contain detrital chlorite and mica. These minerals are absent in the Eocene–early Oligocene sedimentary rocks with the exception of sample PAK 2, which contains white mica.

Heavy minerals. Detrital garnet, tourmaline, staurolite, and aluminosilicates are present in variable proportions in all the analysed samples (i.e. since the early Oligocene; Table 3). Early

Table 2. *Mineralogical composition and relative abundance (*) of analysed mudstones*

Age, sample	Quartz	Calcite	Kaolinite	Smectite	Micas	Chlorite
Early Miocene						
PAK 15	****	**	*	*	*	
PAK 14	****	**	*	*	*	*
Late Oligocene						
PAK 13	****		*	*	*	*
PAK 12	****		*	*		
PAK 11	****		*	*	*	*
PAK 10	****	*	*	*	*	
PAK 7	****	**	*	*	*	
PAK 16	****		*	*	**	*
PAK 9	****		*	*		*
Eocene–Early Oligocene						
PAK 8	****		*	*		
PAK 5		****	*			
PAK 6		****	*			
PAK 4		****	*			
PAK 3	****	**	*	*		
PAK 2	****		*		**	
PAK 1	****	**	*	*		

Table 3. *Heavy mineral identified and their relative abundances*

Age, sample	Garnet	Zircon	Chromite	Tourmaline	Celestine	Staurolite	Epidote	Opaque minerals	Monazite	Aluminosilicate–sillimanite	Apatite	Titanite	Rutile	Amphibole	Pyroxene	Other	Comment
Modern cratonic rivers (Sinha et al. 2009)																	
Chambal (Dholpur)	19 (111)	1 (6)	A	1 (7)	A	1 (4)	15 (91)	14 (82)	2 (9)	4 (26)	1 (6)	1 (6)	0 (1)	38 (230)	2 (13)	1 (8)	
Chambal (Dholpur)	36 (216	1 (8)	A	1 (4)	A	1 (4)	14 (84)	20 (118)	0 (0)	1 (3)	1 (3)	0 (2)	0 (1)	25 (149)	1 (5)	1 (3)	
Betwa (Sohana)	1 (5)	1 (7)	A	0 (0)	A	0 (0)	27 (163)	39 (236)	0 (0)	4 (21)	0 (0)	0 (0)	0 (0)	19 (113)	9 (55)	0 (0)	
Betwa (Sohana)	0 (0)	1 (6)	A	0 (0)	A	0 (0)	24 (142)	67 (400)	0 (0)	0 (0)	0 (0)	0 (2)	0 (0)	8 (50)	0 (0)	0 (0)	
Early Miocene																	
Z-01	16	11	16	16	A	5	16	11	5	5	A	A	A	A	A	A	Increase of epidote
Z-05, Z-08, Z-09, Z-12, Z-14, Z-15	17	11	17	11	A	17	6	11	6	6	A	A	A	A	A	A	Appearance of epidote and decrease of aluminosilicates
Late Oligocene																	
Z-13, Z-17	13	13	13	13	A	13	A	13	13	13	A	A	A	A	A	A	
Z-11	13	13	13	13	A	13	A	13	13	13	A	A	A	A	A	A	Appearance of zircon
Z-06, Z-16	13	A	13	13	13	13	A	13	13	13	A	A	A	A	A	A	
Early Oligocene																	
Z-07	17	A	8	17	17	8	A	A	17	17	A	A	A	A	A	A	Appearance of celestine, monazite and chromite
Z-04, Z-10	22	A	A	22 (?)	A	22	A	11		22	A	A	A	A	A	A	
Z-03	22	A	A	22 (?)	A	22	A	11		22	A	A	A	A	A	A	?Second family of tourmaline with stick shape

For comparison, we calculated percentage (with number of grains counted given in parentheses) of dense minerals from modern cratonic rivers based on data of Sinha *et al.* (2009). For those workers, epidote group includes epidote, zoisite and clinozoisite; sillimanite group includes kyanite and sillimanite; pyroxene group includes augite, with some hypersthene and diopside; opaque minerals group includes hematite, magnetite, goethite, ilmenite and leucoxene; 'others' include olivine, andalusite, chlorite, and unknowns. A, absent.

Oligocene samples Z-03, Z-04, and Z-10 contain stick-shaped tourmaline, which is absent in early Oligocene Z-07 samples and other late Oligocene–Miocene samples (Table 3). Chromite and monazite appear in the late early Oligocene Z-07 sample, stratigraphically the youngest sample before the early–late Oligocene transition (Fig. 4 and Table 3). Chromite content increases throughout the late Oligocene and early Miocene (Table 3). Three samples (Z-07, Z-06 and Z-16) contain celestine (Table 3). Zircon grains were found in the middle part of the late Oligocene sedimentary succession (Z-11) up to the early Miocene (Table 3). Early Miocene samples are characterized by the presence of epidote. The abundance of epidote increases in the late early Miocene (Z-01, Table 3).

Trace element geochemistry and Nd–Sr isotopes of mudstones

The REE contents of the analysed samples were compared with average Post Archaean Australian Shales (PAAS; Taylor & McLennan 1985), which are considered to be representative of the upper continental crust composition.

Eocene–early Oligocene. Compared with PAAS, the Eocene–early Oligocene samples are slightly depleted in light rare earth elements (LREE), enriched in middle rare earth elements (MREE) and depleted in heavy rare earth elements (HREE), and show positive Ce anomalies (Fig. 5). Th, Zr and Hf are depleted relative to PAAS (Table 4) and there are lower Eu anomalies (0.68–0.71) and higher Cr/Th ratios (8–21) than in PAAS. Th/Sc ratios are scattered, ranging from 0.67 (0.7 × PAAS) to 3.68 (4 × PAAS).

The Eocene–early Oligocene samples have εNd(0) values ranging from −8.5 to −9.8. Except for the stratigraphically youngest sample (PAK 8), the $^{87}Sr/^{86}Sr$ ratio varies between 0.708 and 0.712 (Table 5).

Late Oligocene. With the exception of PAK 13, the late Oligocene samples are depleted in REE compared with PAAS (Fig. 5). All of these samples have similar REE patterns with a positive Ce anomaly and enrichment in LREE and MREE compared with HREE (Fig. 5). They are depleted in Zr relative to PAAS (Table 4). They have variable Th/Sc ratios (0.83–1.79), Cr/Th ratios (6–13) and Eu anomalies (0.60–0.73). These ratios are not correlated.

The late Oligocene samples have more negative εNd(0) (−9.9 to −13.3) and more radiogenic $^{87}Sr/^{86}Sr$ ratio (0.712–0.724) than those of Eocene–early Oligocene samples (Table 5 and Fig. 6).

Early Miocene. Compared with PAAS, the early Miocene sedimentary rocks are depleted in LREE and HREE. REE patterns are similar to those of other series, with enrichment in LREE over HREE (Fig. 5). Th, Zr and Hf are depleted relative to PAAS (Table 4), with variable Eu anomalies (0.62–0.69) and Cr/Th ratios (6–11), and similar Th/Sc ratios (1.23 and 1.24). The sample with the highest Eu anomaly (PAK 14) has Th/Sc ratios similar to those of the sample with the lowest Eu anomaly (PAK 15).

PAK 14 has εNd(0) and $^{87}Sr/^{86}Sr$ values similar to those of the late Oligocene samples. PAK 15 records an increase of εNd(0) value associated with a decrease of its $^{87}Sr/^{86}Sr$ ratio.

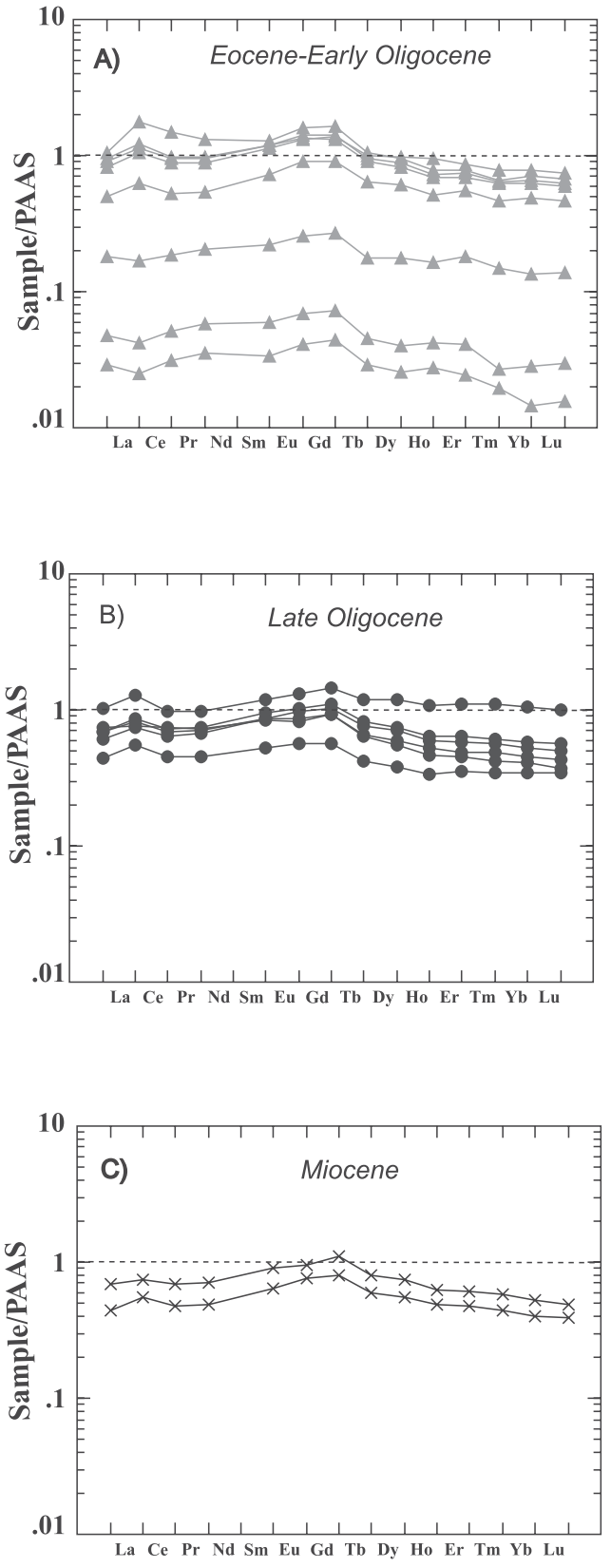

Fig. 5. Concentrations of the REE for Palaeogene to Neogene samples normalized against PAAS (Taylor & McLennan 1985).

Discussion

Provenance of the analysed deposits

REE and Eu anomaly as well as elemental ratios (Cr/Th and Th/Sc) have proven to be useful tools for determining the composition of the source area of sediments (Taylor & McLennan 1985; McLennan *et al.* 1993). Sedimentary processes can modify the chemical composition of mudstones during and after their deposition by favouring the accumulation of heavy minerals such as zircon and monazite. This accumulation in turn can modify the concentrations of certain elements (REE, Th, Zr and Hf) and elementary ratios (Cr/Th, Th/U, Th/Sc) that are classically used to determine the provenance of sediments (McLennan *et al.* 1993). For instance, enrichment in zircon will enrich the sediment in Zr, Hf and HREE, whereas enrichment in monazite will coincide with enrichment in REE (McLennan *et al.* 1993).

All of the analysed sedimentary rocks are depleted in Th, Zr, Hf and HREE relative to PAAS, and they show enrichment in LREE over HREE, which suggests that heavy minerals did not influence the chemical composition of the analysed samples.

The Sr and Nd isotopic compositions of the 16 samples are reported in a εNd(0) v. $^{87}Sr/^{86}Sr$ diagram (Fig. 7). To determine if the samples are consistent with derivation from the Himalaya, we compared our values with Himalayan bedrock and with coeval samples of known Himalayan derivation (Subathu and Post-Subathu deposits of Najman *et al.* (2000) and Bera *et al.* (2010)). Also plotted in Figure 7 are Nd–Sr isotopic compositions of Pleistocene to Holocene Indus-derived sediments (Kessarkar *et al.* 2003). Potential sources for our sedimentary rocks include western Himalayan subunits and the northwestern Indian craton, all defined in Table 6 and mapped in Figure 1.We exclude the Lesser Himalayan rocks because exhumation of this unit started during the late Miocene (12–10 Ma; Huyghe *et al.* (2001) or *c*. 11 Ma (Najman *et al.* 2009), well after the stratigraphically youngest studied sample.

The analysed samples define two distinct groups. The first consists of Eocene–early Oligocene samples and the stratigraphically youngest sample (PAK 15), and is characterized by εNd(0) values less negative than −10 (−8.5 to −9.8; mean *c*. −9.40) and by $^{87}Sr/^{86}Sr$ ranging from 0.708 to 0.718. The second group comprises late Oligocene to early Miocene samples and is characterized by slightly more radiogenic Sr isotopic composition (0.712–0.721; mean *c*. 0.717) and more negative εNd(0) values (−9.9 to −13.2; mean *c*. −11.8).

Provenance of 50–30 Ma sedimentary rocks. Early Oligocene samples Z-03, Z-04 and Z-10 have similar heavy mineral assemblages and are stratigraphically situated between Early Oligocene samples PAK 5 and PAK 8 (Fig. 4). We note a change in heavy mineral assemblage for late Early Oligocene Z-07 sample, stratigraphically situated between PAK 8 and PAK 9 (Fig. 4 and Table 3). We assume that samples PAK 16 and PAK 8 and Z-03, Z-04 and Z-10 have similar provenance because no significant change in their mineralogical or isotopic composition is recorded.

Heavy mineral assemblages of samples Z-03, Z-04 and Z-10 (garnet, staurolite, tourmaline and aluminosilicate) suggest derivation from a metamorphic source. The Indian craton (including Archean Banded Gneiss Complex and the Bundelkhand Complex of the Aravalli belt and Aravalli and Delhi Proterozoic supergroups) contains significant metamorphic rocks and could constitute this metamorphic source. High-grade metamorphic Archaean rocks are characterized by negative εNd(0) values

Table 4. *Major (wt%) and trace elements (ppm) concentrations of the analysed mudstones*

Sample:	PAK 1	PAK 2	PAK 3	PAK 4	PAK 6	PAK 5	PAK 8	PAK 9	PAK 16	PAK 7	PAK 10	PAK 11	PAK 12	PAK 13	PAK 14	PAK 15	PAAS
Type:	Mudstone	Mudstone	Mudstone	Mudstone	Mudstone	Mudstone	Mudstone	Mudstone	Mudstone	Mudstone	Mudstone	Mudstone	Palaeosol	Palaeosol	Mudstone	Mudstone	
wt%																	
SiO_2	56.89	60.12	55.62	23.00	17.54	10.63	69.15	79.10	64.90	60.12	66.23	65.23	90.12	63.24	55.90	50.94	62.8
Al_2O_3	16.13	19.88	19.47	9.10	6.72	4.18	17.91	10.85	20.85	20.11	14.53	19.03	7.93	18.08	15.45	14.41	18.9
Fe_2O_3	8.45	10.71	10.12	4.22	3.34	3.27	3.56	3.22	5.21	8.47	6.71	6.32	1.25	15.02	5.09	7.94	6.5
MnO	0.20	0.04	0.24	0.07	0.08	0.20	0.02	0.01	0.03	0.07	0.16	0.03	0.01	0.25	0.11	0.10	0.11
MgO	3.68	2.70	4.17	3.98	3.36	1.86	1.35	1.95	2.49	4.07	2.92	3.07	0.66	1.27	4.30	5.93	2.2
CaO	8.33	0.14	5.47	37.42	43.64	51.28	0.15	0.60	0.73	3.55	5.41	0.62	0.23	0.60	12.84	11.54	1.3
Na_2O	1.79	1.47	1.29	1.29	0.49	0.10	0.35	1.25	1.25	0.89	2.10	0.45	0.22	0.30	1.22	2.46	1.2
K_2O	3.03	4.48	2.68	0.92	0.68	0.31	2.66	1.47	4.59	3.82	3.05	3.83	0.03	1.41	3.14	2.79	3.7
TiO_2	0.73	0.94	0.87	0.41	0.30	0.19	0.77	0.50	0.55	0.62	0.57	0.67	0.45	0.96	0.46	0.47	1
P_2O_5	1.04	0.41	0.34	0.34	0.37	0.97	0.30	0.14	0.24	0.43	0.41	0.40	0.06	0.38	0.33	0.62	0.16
LOI	0.36	0.15	0.16	18.62	22.53	27.34	0.13	1.02	1.01	0.11	0.09	0.19	0.21	0.35	1.06	3.12	
Total	100.64	101.05	100.43	99.35	99.04	100.32	96.34	100.10	101.86	102.27	102.17	99.84	101.16	101.88	99.89	100.33	
ppm																	
Sc	13.31	16.57	15.97	5.37	1.68	0.94	14.58	8.09	14.15	14.22	9.93	14.03	5.07	14.98	11.29	10.95	
Rb	144.61	212.93	131.01	42.60	33.76	21.72	147.12	89.85	197.19	154.62	119.36	157.15	13.65	111.24	138.38	106.34	160
Cs	7.27	9.44	7.95	3.36	2.57	1.64	8.72	5.38	10.16	11.20	5.94	10.65	1.83	7.87	9.12	4.15	15
Ba	105.90	90.68	103.29	21.37	8.83	5.69	192.32	163.50	544.57	254.42	276.71	307.46	98.48	266.37	317.31	229.74	650
Sr	273.22	155.28	295.87	901.05	668.26	537.74	121.25	178.86	142.35	117.48	115.82	134.21	53.68	347.65	182.37	392.46	200
Th	10.74	11.07	12.16	0.11	0.04	0.02	14.11	9.59	13.39	9.80	11.51	13.04	6.93	16.41	8.02	1.67	14.6
U	2.11	1.49	1.74	1.57	1.91	3.90	3.26	9.24	3.30	1.29	1.79	2.15	1.02	3.25	2.43	1.68	3.1
Y	21.80	16.05	17.39	1.60	0.32	0.20	18.44	6.57	8.98	13.96	12.74	13.30	11.14	25.89	14.98	9.43	27
Zr	138.88	120.75	129.64	30.20	7.00	2.32	99.91	63.17	55.59	66.90	67.39	72.95	65.70	165.05	34.95	29.29	210
Nb	14.38	19.09	16.64	6.50	4.81	3.11	16.46	9.68	12.23	11.04	12.02	12.77	9.50	17.12	9.22	8.59	19
Hf	3.11	2.74	2.79	0.89	0.24	0.09	2.07	1.63	1.34	1.40	1.60	1.88	1.65	4.04	1.02	0.90	5
Cr	154.03	226.98	152.70	86.07	67.63	42.35	147.08	96.94	99.42	154.92	99.51	150.55	76.81	104.70	85.12	145.26	110
Co	22.01	25.70	21.83	10.61	7.43	6.35	15.58	9.03	12.77	18.97	14.39	26.16	9.41	65.35	17.04	19.53	
V	125.20	148.00	135.39	66.54	54.02	35.38	111.67	74.46	136.36	151.68	100.16	139.12	40.75	209.64	132.37	119.30	150
La	31.65	34.36	36.43	6.95	1.84	1.13	40.35	16.77	26.09	19.27	23.04	26.68	28.06	38.99	26.20	17.04	38.2
Ce	84.62	89.62	97.16	13.50	3.37	2.00	139.69	43.64	64.94	49.87	59.61	68.78	60.02	101.32	59.06	44.48	79.6
Pr	7.73	8.34	8.63	1.65	0.46	0.27	13.26	4.02	6.13	4.59	5.66	6.35	6.49	8.65	6.08	4.20	8.83
Nd	30.31	32.52	33.20	6.88	1.97	1.21	44.06	15.41	23.81	18.32	22.55	25.10	24.71	32.77	24.21	16.69	33.9
Sm	6.23	6.53	6.61	1.22	0.33	0.19	7.18	2.94	4.77	4.01	4.84	5.30	4.69	6.56	4.97	3.58	5.55
Eu	1.41	1.46	1.54	0.27	0.07	0.04	1.71	0.61	0.93	0.98	1.06	1.12	0.88	1.40	1.03	0.82	1.08
Gd	6.37	6.09	6.59	1.26	0.34	0.21	7.73	2.61	4.30	4.26	4.84	5.14	4.30	6.81	5.17	3.69	4.66
Tb	0.77	0.71	0.74	0.14	0.04	0.02	0.82	0.32	0.50	0.50	0.60	0.63	0.51	0.92	0.63	0.46	0.774
Dy	4.62	3.80	4.14	0.82	0.19	0.12	4.44	1.81	2.61	2.84	3.28	3.49	2.81	5.53	3.47	2.59	4.68
Ho	0.94	0.68	0.72	0.16	0.04	0.03	0.78	0.34	0.46	0.51	0.59	0.63	0.52	1.07	0.63	0.48	0.991
Er	2.44	1.95	2.11	0.51	0.12	0.07	2.25	1.00	1.29	1.56	1.64	1.82	1.38	3.18	1.75	1.36	2.85
Tm	0.32	0.25	0.26	0.06	0.01	0.01	0.27	0.14	0.17	0.19	0.23	0.25	0.20	0.44	0.23	0.18	0.405
Yb	2.22	1.74	1.85	0.38	0.08	0.04	1.99	0.98	1.16	1.38	1.48	1.62	1.27	2.95	1.50	1.13	2.82
Lu	0.32	0.26	0.27	0.06	0.01	0.01	0.29	0.15	0.16	0.20	0.22	0.24	0.19	0.43	0.21	0.17	0.433
Eu/Eu*	0.68	0.71	0.71	0.67	0.68	0.69	0.70	0.67	0.62	0.73	0.67	0.66	0.60	0.64	0.62	0.69	0.65
Cr/Th	14.34	20.50	12.56	819.32	1845.93	1824.36	10.42	10.10	7.42	15.81	8.64	11.54	11.09	6.38	10.61	86.86	7.53
Th/Sc	0.81	0.67	0.76	0.02	0.02	0.02	0.97	1.19	0.95	0.69	1.16	0.93	1.37	1.10	0.71	0.15	
Rb/Sr	0.53	1.37	0.44	0.05	0.05	0.04	1.21	0.50	1.39	1.32	1.03	1.17	0.25	0.32	0.76	0.27	

PAAS, Post Archaean Australian Shales (Taylor & McLennan 1985). LOI, loss on ignition.

Table 5. *Nd and Sr isotopic compositions in analysed mudstones*

Sample	Sr (ppm)	Nd (ppm)	$^{143}Nd/^{144}Nd$	$\pm 2\sigma$	$\varepsilon Nd(0)$	$^{87}Sr/^{86}Sr$	$\pm 2\sigma$
PAK 15	392.30	16.68	0.512164	7	−9.25	0.711687	9
PAK 14	182.37	24.21	0.512029	6	−11.88	0.716867	10
PAK 13	347.50	32.76	0.512009	9	−12.27	0.713070	10
PAK 12	53.66	24.70	0.512090	9	−10.69	0.711854	9
PAK 11	134.20	25.10	0.512133	8	−9.85	0.717740	9
PAK 10	115.79	22.54	0.512038	8	−11.70	0.721463	10
PAK 7	117.45	18.31	0.511999	7	−12.47	0.717557	8
PAK 16	142.34	23.80	0.511959	6	−13.25	0.724431	8
PAK 9	178.78	15.40	0.512023	7	−12.00	0.712894	9
PAK 8	121.25	44.06	0.512148	7	−9.56	0.718066	8
PAK 5	537.70	1.21	0.512157	9	−9.38	0.708067	11
PAK 6	668.06	1.97	0.512135	15	−9.81	0.708079	17
PAK 4	900.75	6.88	0.512138	8	−9.75	0.708189	16
PAK 3	295.76	33.19	0.512163	10	−9.27	0.710253	8
PAK 2	155.24	32.51	0.512202	8	−8.51	0.712224	11
PAK 1	273.16	30.30	0.512151	6	−9.50	0.710098	9

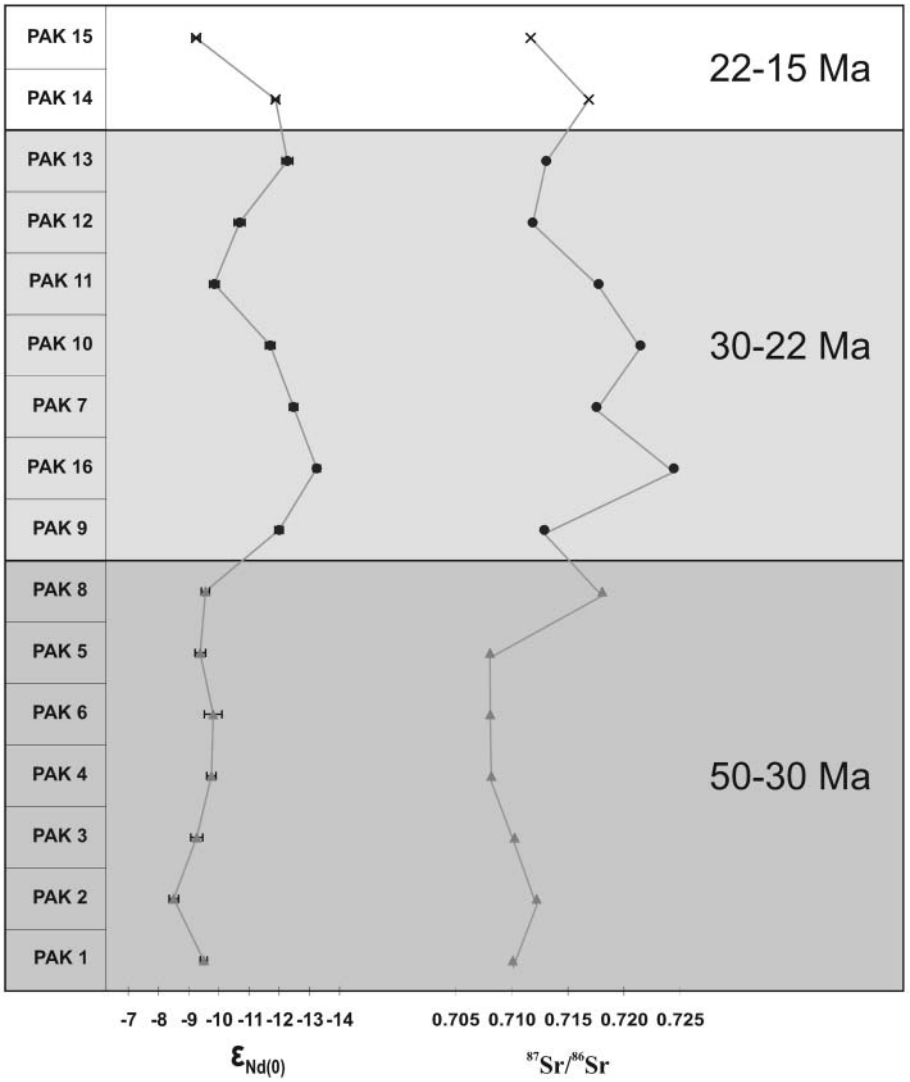

Fig. 6. Stratigraphical variations of $\varepsilon Nd(0)$ and $^{87}Sr/^{86}Sr$ values for analysed samples.

(< -30) and very high radiogenic $^{87}Sr/^{86}Sr$ ratios (>0.800) (Peucat *et al.* 1989; Saha *et al.* 2004; Chakrabarti *et al.* 2007; Najman *et al.* 2008), which is not the case with the Nd–Sr isotopic compositions of the Eocene–early Oligocene sedimentary rocks we analysed. Hence, we dismiss a strictly Archaean source. To our knowledge, no Nd–Sr isotopic composition for the Aravalli and Delhi Proterozoic supergroups is available. However, when compared with $\varepsilon Nd(0)$ values of other Indian shield Proterozoic sedimentary rocks, which are more negative than −13.8 (Table 6), the Eocene–early Oligocene sedimentary

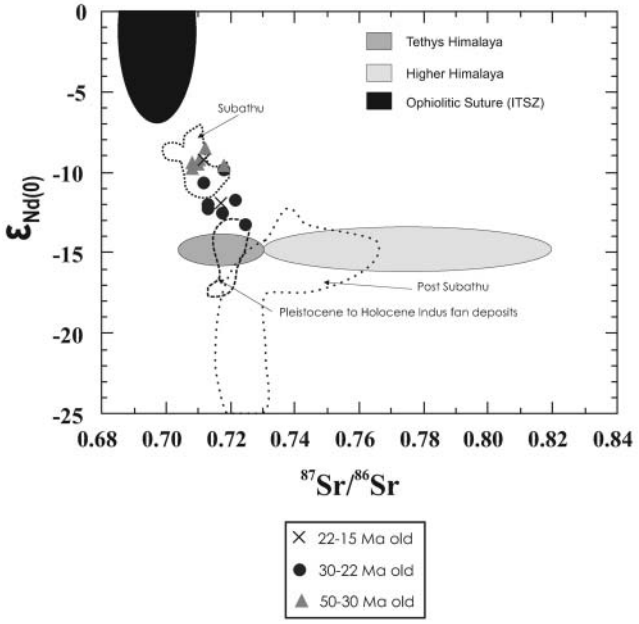

Fig. 7. $^{87}Sr/^{86}Sr$–$\varepsilon Nd(0)$ diagram for analysed sedimentary rocks. ITSZ, Indus–Tsangpo Suture Zone. Data for Indus–Tsangpo Suture Zone, Tethys Himalaya and Higher Himalayan Crystallines fields have been given by Najman (2006). Subathu field includes data from Najman *et al.* (2000) and Bera *et al.* (2010). Post-Subathu field consists of Nd–Sr isotopic composition of basal Dagshai White Sandstones (Bera *et al.* 2010) and Daghsai and Kasauli deposits (Najman *et al.* 2000; Bera *et al.* 2010). Also shown is the field of Indus deposits (Kessarkar *et al.* 2003).

rocks have lower $\varepsilon Nd(0)$ value. These samples have also lower $^{87}Sr/^{86}Sr$ ratio and higher $\varepsilon Nd(0)$ values than that of the modern Daramador cratonic river sand (Table 6). In addition, heavy mineral assemblages of modern rivers (Betwa and Chambal rivers, Table 3) draining the Aravalli belt differ from the Eocene–early Oligocene heavy minerals so far identified. Heavy mineral assemblages of these modern cratonic rivers consist predominantly of amphibole (25–38%), epidote (14–15%), garnet (19–36%) and opaque minerals (14–20%) for the Chambal river, and of amphibole (8–19%), epidote (24–27%) and opaque minerals (39–67%) for the Betwa river (Sinha *et al.* 2009). Zircon is also present in minor quantity (*c*. 1%, Sinha *et al.* 2009). Amphibole, epidote and zircon are lacking in the Eocene–early Oligocene sedimentary rocks. We acknowledge that the lack of unstable species (amphibole, pyroxene) could indicate extensive diagenetic dissolution (Garzanti & Andò 2007) but this is not the case for epidote and zircon. For these reasons, a significant contribution of the Indian shield seems unlikely. Instead, these sedimentary rocks may have an orogenic Himalayan-derived provenance.

Nd–Sr isotopic compositions of the analysed samples plot close to and within the field of the isotopic compositions of the coeval Eocene Subathu Formation (Fig. 7). Based on these Nd–Sr isotopic ratios, Najman *et al.* (2000) suggested a mixed northern provenance with contributions from the Tethys Himalaya and the Indus–Tsangpo Suture Zone (Ophiolitic Suture). However, as our heavy minerals show metamorphic input, this suggests additional contributions of a high- to medium-grade metamorphic source. We dismiss the Higher Himalayan Crystallines as a potential source because of the lack of low-grade metamorphic minerals. If this unit were exposed at that time, its less metamorphosed cover would have already been eroded (e.g. Haimanta), which should be reflected in the mineralogy of the samples we analysed by the presence of low-grade metamorphic minerals. The two sources exposed at that time that are characterized by the occurrence of metamorphic minerals are the North Himalayan gneissic domes and the Karakorum Mountains. $^{40}Ar/^{39}Ar$ and fission-track data show that by 40 Ma, these deep units had already been exhumed (van der Beek *et al.* 2009).

Hence, the potential sources of 50–30 Ma sedimentary rocks are the Karakorum Mountains, the Transhimalaya Zone, the Ophiolitic Suture, the North Himalayan gneissic domes and the Tethys Himalaya. With the identification of these possible sources, it is possible to quantitatively estimate the relative contribution of each of them. Because the North Himalayan gneissic domes comprise metamorphosed sedimentary rocks from the Tethys Himalaya (Guillot *et al.* 2008) and because both types of rocks have similar isotopic compositions (Table 6), we group the North Himalayan gneissic domes and the Tethys Himalaya as a unique end-member, termed hereafter Tethys Himalaya. Simple mixing calculations were performed to evaluate the relative contribution of each of the end-members, namely Karakorum, Ophiolitic suture, Trans-Himalaya, and Tethys Himalaya. The approach was to search for best-fit solutions that would most closely reproduce the Nd isotopic composition expressed as $\varepsilon Nd(0)$ and Nd concentration of each sample and would also yield Sr isotopic composition and Sr concentrations in agreement with our data (Table 7). No perfect match could be obtained, especially for the Sr concentration and isotopic compositions, probably as a result of post-depositional processes and because Sr is sensitive to seasonal variations (Viers *et al.* 2008). The best fit was obtained with major contributions from the Karakorum (40%) and from the Tethys Himalaya (40%) and subordinate contributions from the Ophiolitic Suture (10%) and Trans-Himalaya (10%).

Provenance of 30–22 Ma sedimentary rocks. The early to late Oligocene transition is marked by a shift toward more negative $\varepsilon Nd(0)$ values, an increase in $^{87}Sr/^{86}Sr$ ratios and a strong lowering in REE contents (Tables 4 and 5, Figs 5–7). From a mineralogical point of view, chlorite is present in PAK 9 (late Oligocene sample), whereas it is absent in PAK 8 (early Oligocene sample). These changes are accompanied by a change in heavy mineral assemblages just before the early–late Oligocene transition. Sample Z-07, late early Oligocene in age (*c*. 30 Ma) but stratigraphically between PAK 8 and PAK 9, is characterized by the occurrence of monazite, chromite and celestine but lacks stick-shaped tourmaline.

The shift toward more negative $\varepsilon Nd(0)$ values and more radiogenic $^{87}Sr/^{86}Sr$ ratios could indicate a contribution from Archaean Indian cratonic rocks. However, a significant contribution of the Indian craton can be ruled out as the heavy minerals identified are different from those of Indian cratonic rivers, which consist mainly of epidote, amphibole, garnet and opaque minerals (Table 3; Sinha *et al.* 2009). Rather, more negative $\varepsilon Nd(0)$ values and the appearance of chlorite and monazite suggest the contribution of a new metamorphic source. Similar shift toward more negative $\varepsilon Nd(0)$ values and dominant lithic metamorphic fragments are recorded in the Oligocene Indian foreland deposits of the White Sandstone unit and Dagshai Formation (Najman *et al.* 2000; Bera *et al.* 2010). These are interpreted to document the erosion of either the North Himalayan gneissic domes or the Higher Himalayan Crystallines (Najman *et al.* 2000; Bera *et al.* 2010). Previous studies of Pakistan

Table 6. *Main lithologies, mineralogy and Nd–Sr isotopic compositions of potential sources*

Sources	Units	Main lithologies and characteristics	Mineralogy	εNd(0)	$^{87}Sr/^{86}Sr$	References for Nd–Sr isotopic ratios
Indian Craton						
Precambrian sequences of the Aravalli craton (Ahmad *et al.* 2008, and references therein)	Banded Gneissic Complex basement (3500–2500 Ma)	High-grade metamorphic rocks (granitic gneisses, granitoids, amphibolites and metasediments)		< -25	>0.800	Peucat *et al.* 1989; Saha *et al.* 2004; Najman *et al.* 2008
	Aravalli Supergroup supracrustal rocks (2500–2000 Ma)	Conglomerates, quartzites, metavolcanites, carbonates				
	Delhi Supergroup supracrustal rocks (2000–1700 Ma)	Quartzites, arkoses and conglomerates				
	Basal Aravilli volcanism (2300–1800 Ma)			−12 to −28.1 but most have < -18		Ahmad *et al.* 2008, and references therein
Vindhyan Basin	Bundelkhand granite massif (3300–3200 Ma)			−34		Chakrabarti *et al.* 2007
	Proterozoic Bandher, Rewa, Kaimur and Semri groups	Sandstones and shales		−13.8 to −22 (mean *c.* −17.6; $n = 20$)		Chakrabarti *et al.* 2007
Modern Damodar river sand	Damodar river			−13.8	0.782653	Najman *et al.* 2008
Western Himalaya						
Karakorum mountains	Cretaceous Karakorum batholith	Pre-Miocene Barrovian metamorphism in the Karakorum metamorphic complex (Searle *et al.* 1999)		−7 to −13	0.705–0.720	Mahéo *et al.* 2009
Transhimalaya zone	Kohistan Arc	Cretaceous to Eocene calc-alkaline plutons (Searle *et al.* 1999)		-6.5 ± 2	0.705 ± 0.004	Clift *et al.* 2002; Singh & France-Lanord 2002
Ophiolitic Suture	Ophiolite Belt of Pakistan, Northern Suture, and Indus–Tsangpo Suture Zone	Deep-water Indian sediments, ophiolites, island arc volcanic rocks, forearc sediments and post-early Eocene molasse (Garzanti & Van Haver 1988; Clift *et al.* 2002)		+5 to +13	< 0.710	Mahéo *et al.* 2004; Dhuime *et al.* 2007
North Himalayan gneissic domes	Tso Morari unit	Cambro-Ordovician gneissic basement overlain by an Upper Carboniferous to Permian ultrahigh-pressure metasedimentary cover (Greco *et al.* 1989; de Sigoyer *et al.* 2004); gneissic domes are metamorphosed sediments from the Tethys Himalaya (Guillot *et al.* 2008)	Abundant garnet, micas, kyanite, tourmaline and staurolite (Guillot *et al.* 2008)	−13 to −18	0.728–0.729	de Sigoyer *et al.* 2004
Tethys Himalaya		Late Precambrian to early Permian siliciclastic rocks and carbonates and late Permian to early Eocene shelf carbonates (Critelli & Garzanti 1994)		−7 to −19	0.705–0.750	Najman *et al.* 2000; Robinson *et al.* 2001; Richards *et al.* 2005
Higher Himalayan Crystallines		High-grade metamorphic late Proterozoic and younger Indian continental crust and leucogranites (Parrish & Hodges 1996)		*c.* −15	0.730–0.820	Richards *et al.* 2005; Najman 2006
Lesser Himalaya		Proterozoic metamorphic rocks (DiPietro & Pogue 2004) and low-grade mid-Proterozoic clastic and carbonate sequence (Parrish & Hodges 1996); derivation from the Indian craton (Richards *et al.* 2005)		*c.* −25	0.75 to >0.80	Richards *et al.* 2005

Table 7. *Source composition, samples modelled, mixing parameters and best-fit results for analysed mudstones*

	Nd (ppm)	Sr (ppm)	εNd(0)	$^{87}Sr/^{86}Sr$	References
Sources					
Karakorum–Hindu Kush (Kara)	50	700	−10	0.71	Clift *et al.* 2002; Mahéo *et al.* 2009
Ophiolitic Suture (OS)	5	200	7	0.705	Mahéo *et al.* 2004; Dhuime *et al.* 2007
Transhimalaya (Trans)	30	400	3	0.705	Clift *et al.* 2002; Singh & France-Lanord 2002
Higher Himalayan Crystallines (HHC)	30	70	−15	0.78	Robinson *et al.* 2001; Singh & France-Lanord 2002
Tethys Himalaya–North Himalaya gneissic domes (Tethys)	50	80	−15	0.72	Najman *et al.* 2000; Robinson *et al.* 2001

	Nd (ppm)	Sr (ppm)	εNd(0)	$^{87}Sr/^{86}Sr$	Best fit result				Proportions
					Nd (ppm)	Sr (ppm)	εNd(0)	$^{87}Sr/^{86}Sr$	
Sediments									
Eocene–early Oligocene									
PAK 1	30	273	−9.50	0.710	44	372	−9.00	0.713	40% Kara + 40% Tethys + 10% OS + 10% Trans
PAK 2	33	155	−8.51	0.712	44	372	−9.00	0.713	40% Kara + 40% Tethys + 10% OS + 10% Trans
PAK 3	33	296	−9.27	0.710	44	372	−9.00	0.713	40% Kara + 40% Tethys + 10% OS + 10% Trans
PAK 4	7	901	−9.75	0.708	44	372	−9.00	0.713	Not applicable
PAK 6	2	668	−9.81	0.708	44	372	−9.00	0.713	Not applicable
PAK 5	1	538	−9.38	0.708	44	372	−9.00	0.713	Not applicable
PAK 8	44	121	−9.56	0.718	44	372	−9.00	0.713	40% Kara + 40% Tethys + 10% OS + 10% Trans
Late Oligocene–early Miocene									
PAK 9	15	179	−12.00	0.713	38	176	−11.60	0.741	40% HHC + 35% Tethys + 10% Trans + 5% OS + 10% Kara
PAK 16	24	142	−13.25	0.724	38	98	−13.00	0.746	45% HHC + 45% Tethys + 5% Trans + 5% OS
PAK 7	18	117	−12.47	0.718	37	128	−12.75	0.748	50% HHC + 35% Tethys + 5% Trans + 5% OS + 5% Kara
PAK 10	23	116	−11.70	0.721	38	176	−11.60	0.741	40% HHC + 35% Tethys + 10% Trans + 5% OS + 10% Kara
PAK 11	25	134	−9.85	0.718	33	148	−9.45	0.737	35% HHC + 35% Tethys + 5% Trans + 20% OS + 5% Kara
PAK 12	25	54	−10.69	0.712	37	183	−10.50	0.737	35% HHC + 35% Tethys + 10% Trans + 10% OS + 10% Kara
PAK 13	33	348	−12.27	0.713	38	176	−12.50	0.741	40% HHC + 40% Tethys + 5% Trans + 5% OS + 10% Kara
PAK 14	24	182	−11.88	0.717	40	211	−12.10	0.776	40% HHC + 35% Tethys + 10% Trans + 5% OS + 10% Kara
PAK 15	17	392	−9.25	0.712	34	210	−8.95	0.733	30% HHC + 30% Tethys + 5% Trans + 20% OS + 15% Kara

PAK 4, 5 and 6 were not modelled because of their high carbonate content.

foreland deposits indicated that exhumation of the western Higher Himalayan Crystallines occurred during the early Miocene (Najman *et al.* 2003). Oligocene material was long considered to be absent in the Himalaya foothills, but even so, an exhumation of the Higher Himalayan Crystallines at *c*. 30 Ma is not precluded. Additional evidence for a contribution of the Higher Himalayan Crystallines during the Oligocene includes the overall more radiogenic Sr isotopic composition of the Oligocene samples than those of the 50–30 Ma old sedimentary rocks and the appearance of zircon, which is likely to be related to the exhumation of Higher Himalayan granites and gneisses.

The presence of chromite in Himalayan orogenic-derived detritus is used as an indicator for the exhumation and erosion of ophiolitic rocks (Critelli & Garzanti 1994; Warwick *et al.* 1998). Chromite is abundant at the base of the obducted ophiolites in Northwest Himalaya (Mahéo *et al.* 2004) but also in the Kohistan–Ladakh arc (Khan *et al.* 1989) and in the western ophiolite belt of Pakistan (Bela–Muslim Bagh–Zhob–Waziristan; Arif & Qasim Jan 2006). The appearance of chromite in our late early Oligocene samples suggests deep incision of either the Ophiolitic Suture (Northern Suture, Indus–Tsangpo Suture Zone) or the ophiolite belt of Pakistan.

As for the 50–30 Ma sedimentary rocks, we estimated the relative contribution of potential sources identified for 30–22 Ma samples. Best fits were obtained with a major contribution from the Tethys Himalaya (35–45%) and from the Higher Himalayan Crystallines (35–45%) and a subordinate contribution (10–30%) of the Karakorum, Ophiolitic Suture and Trans-Himalaya (Table 7). We note that using the Nd–Sr isotopic data alone, it is difficult to make a clear distinction between the Higher Himalayan crystallines and their cover (Haimanta, Tethyan Sedimentary Series), so the proportions calculated here should be regarded with caution. Nevertheless, our data clearly record exhumation of the Higher Himalayan Crystallines and/or its cover.

The late Oligocene samples (PAK 11 and PAK 12) have higher εNd(0) values, close to those found for the Eocene–early Oligocene group. We have no definite explanation for these samples because this change is not recorded by the mineralogy.

Provenance of 22–15 Ma sedimentary rocks. No major change in provenance indicators is found between the 30–22 Ma sedimentary rocks and the 22–15 Ma samples except for the appearance of epidote. Heavy minerals of the latter samples are garnet, zircon, tourmaline, staurolite, epidote, monazite, and chromite. Associations of garnet, epidote, tourmaline, staurolite, and zircon were found in the late Oligocene–early Miocene Himalayan foreland deposits and were interpreted as sourced in the Higher Himalayan Crystallines (Singh *et al.* 2004). The two analysed samples of this formation show contrasting Nd–Sr isotopic compositions (Figs 5 and 6). The oldest sample (PAK 14) has a Nd–Sr isotopic composition similar to those of the late Oligocene group, whereas the youngest one (PAK 15) displays Eocene–early Oligocene isotopic characteristics (Figs 5 and 6). Because PAK 14 has similar isotopic and mineralogy to late Oligocene samples, we suggest that it had a similar provenance. We have no definite explanation for the lower εNd(0) values and less radiogenic $^{87}Sr/^{86}Sr$ ratios of sample PAK 15. Further sampling is needed to explore whether this sample is representative of a change in provenance.

A scenario for the evolution of the Indus drainage basin during the Palaeogene

The course of the lower reaches of the Indus River during the Palaeogene remains controversial; in particular, the emplacement of the Palaeo-Indus delta–fan complex and its onshore connection. Two loci have been proposed for the emplacement of the delta–fan complex. Based on the thickness and the 'Himalayan' sedimentary provenance of the Khojak Formation, Qayyum *et al.* (1996, 2001) suggested that the Palaeogene delta–fan complex (termed the Khojak fan) was preserved as the Palaeogene Khojak Formation in the Katawaz Basin and eastern Makran. Accessory minerals of the Palaeogene Khojak Formation do not indicate a metamorphic source, in contrast to the data presented in this study. This would suggest that sediments of the Sulaiman fold and thrust belt in Pakistan were not part of the Katawaz drainage system. Because 35% of the Indus fan sediments are estimated to predate the Miocene, Clift *et al.* (2001*b*) proposed that the locus of the Indus fan has remained unchanged since the Palaeogene. The sedimentary rocks analysed by Clift *et al.* (2001*b*) have εNd(0) values and K-feldspar Pb isotopic compositions similar to those of the Pleistocene Indus fan, which led those researchers to assume that they have similar provenance and that the Indus River initiated during Eocene times. The heavy mineral assemblage of Palaeogene Indus fan requires the contribution of metamorphic and igneous rocks (Najman 2006). None of the coeval shallow marine or deltaic formations of Pakistan and India have a significant metamorphic source, with the exception of the 50–30 Ma samples, which suggest that these shallow-marine to deltaic sediments could be the coastal record of the metamorphic source found in the Palaeogene Indus fan. However, this is unlikely, as Palaeogene Indus fan sedimentary rocks have εNd(0) values that are less negative, so that the 50–30 Ma samples cannot be the only source. As the studied rocks have a provenance that differs from coeval Indian and Pakistan (including Katawaz) sedimentary rocks, we propose that during the Eocene–early Oligocene, the palaeogeography of western Himalaya was characterized by two fan systems: (1) the Khojak delta–fan complex and (2) the Indus fan, the latter comprising at least three deltas as recorded by the Indian Subathu, Pakistan Ghazij and the Sulaiman fold and thrust belt sedimentary rocks (Fig. 8). However, to account for negative εNd(0) values of Palaeogene Indus fan sedimentary rocks, an additional drainage system eroding Himalayan rocks with more negative εNd(0) values than those of the Subathu and the samples of this study has yet to be discovered, and precise connections between these deltas and the Palaeogene Indus fan remain unclear (Fig. 8)

Our data recorded a change in provenance at *c*. 30 Ma with exhumation of the proto-Higher Himalaya. A wet tropical climate prevailed during the Eocene–early Oligocene (De Franceschi *et al.* 2008). Hence, it is likely that exhumation and erosion occurred simultaneously. Exhumation of the Higher Himalaya is also recorded by the deposits of the Indian Oligocene White Sandstone unit and Daghsai formation (Najman 2006; Bera *et al.* 2010). This exhumation of the Higher Himalaya could also be responsible for the major influx of metamorphic source found in the coeval Oligo-Miocene Pakistan Murree deposits (Najman 2006). Overall, all the available provenance indicators document increased erosion from the metamorphosed proto-Higher Himalayan range. Because the Late Oligocene to early Miocene Indus fan deposits have similar εNd(0) values to our 30–22 Ma sedimentary rocks (mean εNd(0) *c*. −11.5 and *c*. −11.75 respectively) and because these fluvial deposits recorded fluvial systems that were flowing toward the south (i.e. toward the Indus fan), we suggest that our 30–22 Ma sedimentary rocks are the onshore record of the Indus fan. As other coeval deposits of India and Pakistan are fluvial deposits and recorded a similar change in provenance to our studied rocks, we postulate that they were part of the same drainage system, which was the Palaeo-Indus basin.

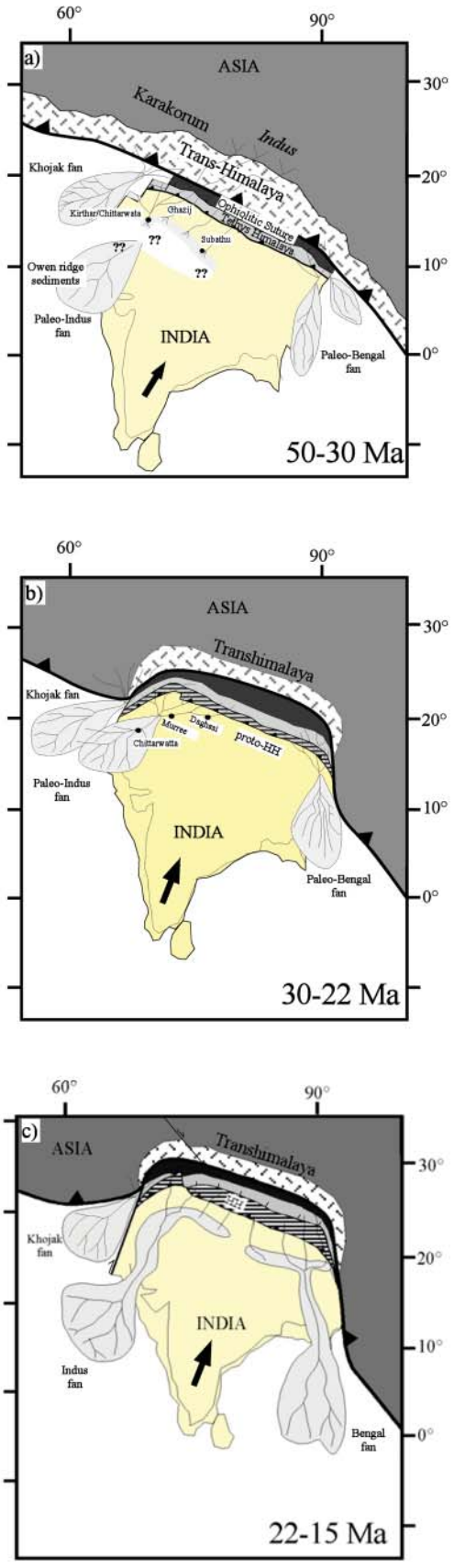

If correct, this suggests that the modern Indus drainage basin is no younger than 30 Ma (Fig. 8). Finally, as the provenance of 22–15 Ma samples is the same as that of the 30–22 Ma sedimentary rocks, we suggest that no major change occurred in the palaeogeography of the western Himalaya between 30 and 15 Ma (Fig. 8).

Conclusion

The studied 50–30 Ma sedimentary rocks are characterized by a mixed orogenic provenance with a major contribution from the Karakorum (40%) and the Tethys Himalaya (40%) and subordinate contributions from the Ophiolitic Suture (10%) and Trans-Himalaya (10%). Heavy mineral assemblages are characterized by the presence of metamorphic minerals. The provenance of our 50–30 Ma samples is distinct from that of the coeval Subathu, Khojak and Ghazij shallow marine formations, which suggests distinct drainage basins. The presence of metamorphic minerals in the heavy mineral assemblages indicates that this drainage basin could be one of the sources that fed the Palaeogene Indus fan. Hence, we propose that during Eocene–early Oligocene time, the palaeogeography of the western Himalaya was characterized by two fans, the Khojak fan and the Indus fan, the latter being fed by at least three deltas.

We document a strong change in provenance that occurred before the early–late Oligocene transition at *c*. 30 Ma. This change in provenance is marked by the appearance of chlorite and monazite and a shift toward more radiogenic Nd–Sr isotopic compositions. We interpret this change as the result of the exhumation and erosion of the proto-Higher Himalaya. The 30–22 Ma sampled rocks are characterized by a major contribution from the Tethys Himalaya (35–45%) and the Higher Himalayan Crystallines (35–45%) and a subordinate contribution (10–30%) from the Karakorum, Ophiolitic Suture and Trans-Himalaya. The provenance of the 22–15 Ma sedimentary rocks is similar to that of the 30–22 Ma samples. As the εNd(0) values of our 30–15 Ma samples are similar to those of the Palaeo-Indus fan deposits, we suggest that the 30–15 Ma sedimentary rocks of the Sulaiman fold and thrust belt were the fluvial onshore record of the Indus fan. As coeval deposits of India and Pakistan recorded similar increasing exhumation of the Higher Himalaya range, we postulate that these sedimentary rocks all derived from the Palaeo-Indus drainage basin. If correct, the modern Indus drainage basin is no younger than 30 Ma.

We are grateful to the late Nawab Akbar Shahbaz Khan Bugti (Dera Bugti), K. Madjidulah (Karachi), N. Iqbal and G. Roohi (Islamabad) for their constant support. We thank J.-L. Welcomme, G. Métais,

Fig. 8. Palaeogeographical maps in a fixed Eurasia reference frame showing the evolution of the Indus and Ganges drainage systems from the Eocene to the early Miocene. (**a**) Reconstruction for 50–30 Ma showing the transition from subduction to collision of the Indian plate beneath the Trans-Himalaya. At that time, only the Ophiolitic Suture and the Tethys Himalaya including the North Himalayan gneissic domes are exhumed and partly eroded, infilling the Khojak and the Palaeo-Indus fan in western Himalaya. The Palaeo-Indus fan comprised at least three deltas as recorded by the Indian Subathu, Pakistan Ghazij and our samples (Kirthar–Chitarwata) although the connections between these deltas and the Palaeogene Indus fan remain unclear. (**b**) Reconstruction for 30–22 Ma. Exhumation of the proto-Higher Himalayan (HH) at *c*. 30 Ma drove drainage reorganization and initiated the modern Indus drainage basin. (**c**) Reconstruction for 22–15 Ma. No major drainage changes occurred. HH, Higher Himalaya.

L. Marivaux, D. De Franceschi and J.-Y. Crochet for their participation in the 2004 fieldwork. S.G. warmly acknowledges Y. Najman for reviewing a first draft of this paper and for her constructive remarks. We thank P. de Parseval, C. Boucayrand, F. Candaudap and P. Brunet for help in heavy mineral analysis and ICP-MS and TIMS measurements. Reviews by Y. Najman, D. Robinson and S. Johnston on an earlier version of this paper were greatly appreciated and helped improve the clarity and the content of the paper. This paper has also benefited from the thoughtful and constructive reviews provided by E. Garzanti and an anonymous reviewer. We thank A. Carter for his helpful editorial handling. The French Ministry of Foreign Affairs, the CNRS (Eclipse-Programme), and the French ANR-ERC PALASIAFRICA Programme (ANR-08-JCJC-0017-01) have financially supported this project.

References

Adnet, S., Antoine, P.O., Hassan Baqri, S.R., Crochet, J.Y., Marivaux, L., Welcomme, J.L. & Métais, G. 2007. New tropical carcharhinids (chondrichthyes, carcharhiniformes) from the late Eocene–early Oligocene of Balochistan, Pakistan: Paleoenvironmental and paleogeographic implications. *Journal of Asian Earth Sciences*, **30**, 303–323.

Ahmad, T., Dragusanu, C. & Tanaka, T. 2008. Provenance of Proterozoic Basal Aravalli mafic volcanic rocks from Rajasthan, Northwestern India: Nd isotopes evidence for enriched mantle reservoirs. *Precambrian Research*, **162**, 150–159.

Allemann, F. 1979. Time of emplacement of the Zhob Valley ophiolites and Bela ophiolites, Baluchistan (preliminary report). *In:* Farah, A. & De Jong, K. A. (eds) *Geodynamics of Pakistan*. Geological Survey of Pakistan, Quetta, 215–242.

Antoine, P.O., Ducrocq, S., Marivaux, L., Chaimanee, Y., Crochet, J.Y., Jaeger, J.J. & Welcomme, J.L. 2003. Early rhinocerotids (Mammalia: Perissodactyla) from South Asia and a review of the Holarctic Paleogene rhinocerotid record. *Canadian Journal of Earth Sciences*, **40**, 365–374.

Antoine, P.-O., Ibrahim Shah, S.M., *et al.* 2004. New remains of the baluchithere *Paraceratherium bugtiense* (Pilgrim 1910) from the Late/latest Oligocene of the Bugti hills, Balochistan, Pakistan. *Journal of Asian Earth Sciences*, **24**, 71–77.

Antoine, P.-O., Downing, K.F., *et al.* 2010. A revision of *Aceratherium blanfordi* Lydekker, 1884 (Mammalia: Rhinocerotidae) from the early Miocene of Pakistan: postcranials as a key. *Zoological Journal of the Linnean Society*, **160**, 139–194.

Arif, M. & Qasim Jan, M. 2006. Petrotectonic significance of the chemistry of chromite in the ultramafic–mafic complexes of Pakistan. *Journal of Asian Earth Sciences*, **27**, 628–646.

Banks, C.J. & Warburton, J. 1986. 'Passive-roof' duplex geometry in the frontal structures of the Kirthar and Sulaiman mountain belts, Pakistan. *Journal of Structural Geology*, **8**, 229–237.

Beck, R.A., Burbank, D.W., *et al.* 1995. Stratigraphic evidence for an early collision between northwest India and Asia. *Nature*, **373**, 55–58.

Bera, M.K., Sarkar, A., Chakraborty, P.P., Loyal, R.S. & Sanyal, P. 2008. Marine to continental transition in Himalayan foreland. *Geological Society of America Bulletin*, **120**, 1214–1232.

Bera, M.K., Sarkar, A., Chakraborty, P.P., Ravikant, V. & Choudhury, A.K. 2010. Forced regressive shoreface sandstone from Himalayan foreland: Implications to early Himalayan tectonic evolution. *Sedimentary Geology*, **229**, 268–281.

Bernet, M., van der Beek, P., Pik, R., Huyghe, P., Mugnier, J.-L., Labrin, E. & Szulc, A. 2006. Miocene to Recent exhumation of the central Himalaya determined from combined detrital zircon fission-track and U/Pb analysis of Siwalik sediments, western Nepal. *Basin Research*, **18**, 393–412.

Blanford, W.T. 1879. *The geology of Sindh*. Memoirs of the Geological Survey of India, **18**.

Bossart, P. & Ottiger, R. 1989. Rocks of the Murree formation in Northern Pakistan: Indicators of a descending foreland basin of late Palaeocene to middle Eocene age. *Eclogae Geologicae Helvetiae*, **82**, 133–165.

Burbank, D.W. 1992. Causes of recent Himalayan uplift deduced from deposited patterns in the Ganges basin. *Nature*, **357**, 680–683.

Burbank, D.W., Derry, L.A. & France-Lanord, C. 1993. Reduced Himalayan sediment production 8 Myr ago despite an intensified monsoon. *Nature*, **364**, 48–50.

Burbank, D.W., Beck, R.A. & Mulder, T. 1996. The Himalayan Foreland. *In:* An, Y. & Harrison, M. (eds) *Asian Tectonics*. Cambridge University Press, Cambridge, 149–188.

Carter, A., Najman, Y., Bahroudi, A., Bown, P., Garzanti, E. & Lawrence, R.D. 2010. Locating earliest records of orogenesis in western Himalaya: Evidence from Paleogene sediments in the Iranian Makran region and Pakistan Katawaz basin. *Geology*, **38**, 807–810.

Chakrabarti, R., Basu, A.R. & Chakrabarti, A. 2007. Trace element and Nd-isotopic evidence for sediment sources in the mid-Proterozoic Vindhyan Basin, central India. *Precambrian Research*, **159**, 260–274.

Clift, P.D. & Blusztajn, J. 2005. Reorganization of the western Himalayan river system after five million years ago. *Nature*, **438**, 1001–1003.

Clift, P.D., Shimizu, N., Layne, G.D. & Blusztajn, J. 2001*a*. Tracing patterns of erosion and drainage in the Paleogene Himalaya through ion probe Pb isotope analysis of detrital K-feldspars in the Indus Molasse, India. *Earth and Planetary Science Letters*, **188**, 475–491.

Clift, P.D., Shimizu, N., *et al.* 2001*b*. Development of the Indus Fan and its significance for the erosional history of the Western Himalaya and Karakoram. *Geological Society of America Bulletin*, **113**, 1039–1051.

Clift, P.D., Carter, A., Krol, M. & Kirby, E. 2002. Constraints on India–Eurasia collision in the Arabian Sea region taken from the Indus Group, Ladakh Himalaya, India. *In:* Clift, P.D., Kroon, D., Craig, J. & Gaedicke, C. (eds) *The Tectonic and Climatic Evolution of the Arabian Sea Region*. Geological Society, London, Special Publications, **195**, 97–116.

Critelli, S. & Garzanti, E. 1994. Provenance of the Lower Tertiary Murree redbeds (Hazara–Kashmir Syntaxis, Pakistan) and initial rising of the Himalayas. *Sedimentary Geology*, **89**, 265–284.

DeCelles, P.G., Gehrels, G.E., Quade, J. & Ojha, T.P. 1998. Eocene–early Miocene foreland basin development and the history of Himalayan thrusting, western and central Nepal. *Tectonics*, **17**, 741–765.

DeCelles, P.G., Gehrels, G.E., Najman, Y., Martin, A.J., Carter, A. & Garzanti, E. 2004. Detrital geochronology and geochemistry of Cretaceous–early Miocene strata of Nepal: implications for timing and diachroneity of initial Himalayan orogenesis. *Earth and Planetary Science Letters*, **227**, 313–330.

De Franceschi, D., Hoorn, C., *et al.* 2008. Floral data from the mid-Cenozoic of central Pakistan. *Review of Palaeobotany and Palynology*, **150**, 115–129.

de Sigoyer, J., Guillot, S. & Dick, P. 2004. Exhumation of the ultrahigh-pressure Tso Morari unit in eastern Ladakh (NW Himalaya): A case study. *Tectonics*, **23**, doi:10.1029/2002TC001492.

Dhuime, B., Bosch, D., Bodinier, J.L., Garrido, C.J., Bruguier, O., Hussain, S.S. & Dawood, H. 2007. Multistage evolution of the Jijal ultramafic–mafic complex (Kohistan, N Pakistan): Implications for building the roots of island arcs. *Earth and Planetary Science Letters*, **261**, 179–200.

DiPietro, J.A. & Pogue, K.R. 2004. Tectonostratigraphic subdivisions of the Himalaya: A view from the west. *Tectonics*, **23**, paper number TC5001.

Downing, K.F. & Lindsay, E.H. 2005. Relationship of Chitarwata formation paleodrainage and paleoenvironments to Himalayan tectonics and Indus river paleogeography. *Paleontologia Electronica*, **8**, 20A.

Downing, K.F., Lindsay, E.H., Downs, W.R. & Speyer, S.E. 1993. Lithostratigraphy and vertebrate biostratigraphy of the Early Miocene Himalayan Foreland, Zinda Pir Dome, Pakistan. *Sedimentary Geology*, **87**, 25–37.

France-Lanord, C. & Derry, L.A. 1997. Organic carbon burial forcing of the carbon cycle from Himalayan erosion. *Nature*, **390**, 65–67.

Friedman, R., Gee, J., Tauxe, L., Downing, K. & Lindsay, E. 1992. The magnetostratigraphy of the Chitarwata and lower Vihowa formations of the Dera Ghazi Khan area, Pakistan. *Sedimentary Geology*, **81**, 253–268.

Garzanti, E. & Andò, S. 2007. Heavy-mineral concentration in modern sands: Implications for provenance interpretation. *In:* Mange, M. & Wright, D. (eds) *Heavy Minerals in Use*. Developments in Sedimentology, **58**, 517–545.

Garzanti, E. & Van Haver, T. 1988. The Indus clastics: forearc basin sedimentation in the Ladakh Himalaya (India). *Sedimentary Geology*, **59**, 237–249.

Garzanti, E., Critelli, S. & Ingersoll, R.V. 1996. Paleogeographic and paleotectonic evolution of the Himalayan Range as reflected by detrital modes of Tertiary sandstones and modern sands (Indus transect, India and Pakistan). *Geological Society of America Bulletin*, **108**, 631–642.

Gingerich, P.D., Russell, D.E., *et al.* 1979. Reconnaissance survey and vertebrate paleontology of some Paleocene and Eocene formations in Pakistan. *University of Michigan Contributions of the Museum of Paleontology*, **25**, 105–116.

Gnos, E., Immenhauser, A. & Peters, T. 1997. Late Cretaceous/early Tertiary convergence between the Indian and Arabian plates recorded in ophiolites and related sediments. *Tectonophysics*, **271**, 1–19.

Gradstein, F. & Ogg, J. 2006. TS-Creator (c)—Chronostratigraphic data base and visualisation: Cenozoic–Mesozoic–Paleozoic integrated stratigraphy and user-generated time scale graphics and charts. *Geoarabia*, **11**, 181–184.

Greco, A., Martinotti, G., Papritz, K., Ramsay, G.J. & Rey, R. 1989. The crystalline rocks of the Kaghan Valley (NE Pakistan). *Eclogae Geologicae Helvetiae*, **82**, 629–653.

Guillot, S., Mahéo, G., de Sigoyer, J., Hattori, K.H. & Pêcher, A. 2008. Tethyan and Indian subduction viewed from the Himalayan high- to ultrahigh-pressure metamorphic rocks. *Tectonophysics*, **451**, 225–241.

Hay, W.W. 1998. Detrital sediment fluxes from continents to oceans. *Chemical Geology*, **145**, 287–323.

Huyghe, P., Galy, A., Mugnier, J.-L. & France-Lanord, C. 2001. Propagation of the thrust system and erosion in the Lesser Himalaya: Geochemical and sedimentological evidence. *Geology*, **29**, 1007–1010.

Jacobsen, S.B. & Wasserburg, G.J. 1980. Sm–Nd isotopic evolution of chondrites. *Earth and Planetary Science Letters*, **50**, 139–155.

Jadoon, I.A.K. & Khurshid, A. 1996. Gravity and tectonic model across the Sulaiman fold belt and the Chaman fault zone in western Pakistan and eastern Afghanistan. *Tectonophysics*, **254**, 89–109.

Jadoon, I.A., Lawrence, R.D. & Lillie, R. J. 1994*a*. Seismic data, geometry, evolution, and shortening in the active Sulaiman fold-and-thrust belt of Pakistan, southwest of the Himalayas. *AAPG Bulletin*, **78**, 758–774.

Jadoon, I.A.K., Lawrence, R.D. & Shahid Hassan, K. 1994*b*. Mari–Bugti pop-up zone in the central Sulaiman fold belt, Pakistan. *Journal of Structural Geology*, **16**, 147–158.

Johnson, N.M., Stix, J., Tauxe, L., Cerveny, P.F. & Tahirkheli, R.A.K. 1985. Paleomagnetic chronology, fluvial processes, and tectonic implications of the Siwalik Deposits near Chinji Village, Pakistan. *Journal of Geology*, **93**, 27–40.

Kessarkar, P.M., Rao, V.P., Ahmad, S.M. & Babu, G.A. 2003. Clay minerals and Sr–Nd isotopes of the sediments along the western margin of India and their implication for sediment provenance. *Marine Geology*, **202**, 55–69.

Khan, M.A., Jan, M.Q., Windley, B.F., Tarney, J. & Thirlwall, M.F. 1989. The Chilas mafic–ultramafic igneous complex; the root of the Kohistan island arc in the Himalaya of northern Pakistan. *In:* Malinconico, L.M. & Lillie, R.J. (eds) *Tectonics of the Western Himalayas*. Geological Society of America, Special Papers, **232**, 75–94.

Kidd, R.B. & Davies, T.A. 1978. Indian Ocean sediment distribution since the Late Jurassic. *Marine Geology*, **26**, 49–70.

Lindsay, E.H., Flynn, L.J., Cheema, I.U., Barry, J.C., Downing, K.F., Rajpar, A.R. & Raza, S.M. 2005. Will Downs and the Zinda Pir Dome. *Palaeontologia Electronica*, **8**, 19A.

Mahéo, G., Bertrand, H., Guillot, S., Villa, I.M., Keller, F. & Capiez, P. 2004. The South Ladakh ophiolites (NW Himalaya, India): an intra-oceanic tholeiitic arc origin with implication for the closure of the Neo-Tethys. *Chemical Geology*, **203**, 273–303.

Mahéo, G., Blichert-Toft, J., Pin, C., Guillot, S. & Pecher, A. 2009. Partial melting of mantle and crustal sources beneath South Karakorum, Pakistan: implications for the Miocene geodynamic evolution of the India–Asia convergence zone. *Journal of Petrology*, **50**, 427–449.

McLennan, S.M., Hemming, S., McDaniel, D.K. & Hanson, G.N. 1993. Geochemical approaches to sedimentation, provenance, and tectonics. *In:* Johnsson, M.J. & Basu, A. (eds) *Processes Controlling the Composition of Clastic Sediments*. Geological Society of America, Special Papers, **284**, 21–40.

Métais, G., Antoine, P.-O., Baqri, S.R.H., Crochet, J.-Y., De Franceschi, D., Marivaux, L. & Welcomme, J.-L. 2009. Lithofacies, depositional environments, regional biostratigraphy and age of the Chitarwata Formation in the Bugti Hills, Balochistan, Pakistan. *Journal of Asian Earth Sciences*, **34**, 154–167.

Najman, Y. 2006. The detrital record of orogenesis: A review of approaches and techniques used in the Himalayan sedimentary basins. *Earth-Science Reviews*, **74**, 1–72.

Najman, Y. & Garzanti, E. 2000. Reconstructing early Himalayan tectonic evolution and paleogeography from Tertiary foreland basin sedimentary rocks, northern India. *Geological Society of America Bulletin*, **112**, 435–449.

Najman, Y.M.R., Pringle, M.S., Johnson, M.R.W., Robertson, A.H.F. & Wijbrans, J.R. 1997. Laser $^{40}Ar/^{39}Ar$ dating of single detrital muscovite grains from early foreland-basin sedimentary deposits in India: Implications for early Himalayan evolution. *Geology*, **25**, 535–538.

Najman, Y., Bickle, M. & Chapman, H. 2000. Early Himalayan exhumation: Isotopic constraints from the Indian foreland basin. *Terra Nova*, **12**, 28–34.

Najman, Y., Garzanti, E., Pringle, M., Bickle, M., Stix, J. & Khan, I. 2003. Early–Middle Miocene paleodrainage and tectonics in the Pakistan Himalaya. *Geological Society of America Bulletin*, **115**, 1265–1277.

Najman, Y., Johnson, K., White, N. & Oliver, G. 2004. Evolution of the Himalayan foreland basin, NW India. *Basin Research*, **16**, 1–24.

Najman, Y., Bickle, M., *et al.* 2008. The Paleogene record of Himalayan erosion: Bengal Basin, Bangladesh. *Earth and Planetary Science Letters*, **273**, 1–14.

Najman, Y., Bickle, M., *et al.* 2009. Reconstructing the exhumation history of the Lesser Himalaya, NW India, from a multitechnique provenance study of the foreland basin Siwalik Group. *Tectonics*, **28**, paper number TC5018.

Parrish, R.R. & Hodges, V. 1996. Isotopic constraints on the age and provenance of the Lesser and Greater Himalayan sequences, Nepalese Himalaya. *Geological Society of America Bulletin*, **108**, 904–911.

Peucat, J.J., Vidal, P., Bernard-Griffiths, J. & Condie, K.C. 1989. Sr, Nd and Pb isotopic systematics in the Archaean low-to-high-grade transition zone of southern India: syn-accretion granulites. *Journal of Geology*, **97**, 537–550.

Pivnik, D.A. & Wells, N.A. 1996. The transition from Tethys to the Himalaya as recorded in northwest Pakistan. *Geological Society of America Bulletin*, **108**, 1295–1313.

Qayyum, M., Niem, A.R. & Lawrence, R.D. 1996. Newly discovered Paleogene deltaic sequence in Katawaz basin, Pakistan, and its tectonic implications. *Geology*, **24**, 835–838.

Qayyum, M., Lawrence, R.D. & Niem, A.R. 1997. Discovery of the palaeo-Indus delta–fan complex. *Journal of the Geological Society, London*, **154**, 753–756.

Qayyum, M., Niem, A.R. & Lawrence, R.D. 2001. Detrital modes and provenance of the Paleogene Khojak Formation in Pakistan: Implications for early Himalayan orogeny and unroofing. *Geological Society of America Bulletin*, **113**, 320–332.

Raymo, M.E. & Ruddiman, W.F. 1992. Tectonic forcing of late Cenozoic climate. *Nature*, **359**, 117–122.

Richards, A., Argles, T., Harris, N., Parrish, R., Ahmad, T., Darbyshire, F. & Draganits, E. 2005. Himalayan architecture constrained by isotopic tracers from clastic sediments. *Earth and Planetary Science Letters*, **236**, 773–796.

Robinson, D.M., DeCelles, P.G., Patchett, P.J. & Garzione, C.N. 2001. The kinematic evolution of the Nepalese Himalaya interpreted from Nd isotopes. *Earth and Planetary Science Letters*, **192**, 507–521.

Roddaz, M., Viers, J., Brusset, S., Baby, P. & Herail, G. 2005. Sediment provenances and drainage evolution of the Neogene Amazonian foreland basin. *Earth and Planetary Science Letters*, **239**, 57–78.

Roddaz, M., Viers, J., Brusset, S., Baby, P., Boucayrand, C. & Herail, G. 2006. Controls on weathering and provenance in the Amazonian foreland basin: Insights from major and trace element geochemistry of Neogene Amazonian sediments. *Chemical Geology*, **226**, 31–65.

Saha, A.R., Basu, A., Garzione, C.N., Bandyopadhyay, P.K. & Chakrabarti, A. 2004. Geochemical and petrological evidence for subduction–accretion processes in the Archean Eastern Indian Craton. *Earth and Planetary Science Letters*, **220**, 91–106.

Searle, M.P., Asif Khan, M., Fraser, J.E. & Gough, S.J. 1999. The tectonic evolution of the Kohistan–Karakoram collision belt along the Karakoram highway transect, north Pakistan. *Tectonics*, **18**, 929–949.

Shah, I. 1977. *Stratigraphy of Pakistan*. Memoirs of the Geological Survey of Pakistan, 12.

Sinclair, H.D. & Jaffey, N. 2001. Sedimentology of the Indus Group, Ladakh, northern India: implications for the timing of initiation of the palaeo-Indus River. *Journal of the Geological Society, London*, **158**, 151–162.

Singh, B.P., Pawar, J.S. & Karlupia, S.K. 2004. Dense mineral data from the northwestern Himalayan foreland sedimentary rocks and recent river sediments: evaluation of the hinterland. *Journal of Asian Earth Sciences*, **23**, 25–35.

Singh, S.K. & France-Lanord, C. 2002. Tracing the distribution of erosion in the Brahmaputra watershed from isotopic compositions of stream sediments. *Earth and Planetary Science Letters*, **202**, 645–662.

Sinha, R., Kettanah, Y., *et al.* 2009. Craton-derived alluvium as a major sediment source in the Himalayan Foreland Basin of India. *Geological Society of America Bulletin*, **121**, 1596–1610.

Summerfield, M.A. & Hulton, N.J. 1994. Natural controls of fluvial denudation rates in major world drainage basins. *Journal of Geophysical Research*, **99**, 13871–13883.

Taylor, S.R. & McLennan, S.M. 1985. *The Continental Crust: Its Composition and Evolution*. Blackwell, Oxford.

van der Beek, P., Robert, X., Mugnier, J.-L., Bernet, M., Huyghe, P. & Labrin, E. 2006. Late Miocene–Recent exhumation of the central Himalaya and recycling in the foreland basin assessed by apatite fission-track thermochronology of Siwalik sediments, Nepal. *Basin Research*, **18**, 413–434.

van der Beek, P., Van Melle, J., Guillot, S., Pecher, A., Reiners, P.W., Nicolescu, S. & Latif, M. 2009. Eocene Tibetan plateau remnants preserved in the northwest Himalaya. *Nature Geoscience*, **2**, 364–368.

Viers, J., Roddaz, M., *et al.* 2008. Seasonal and provenance controls on Nd–Sr isotopic compositions of Amazon rivers suspended sediments and implications for Nd and Sr fluxes exported to the Atlantic Ocean. *Earth and Planetary Science Letters*, **274**, 511–523.

Waheed, A. & Wells, N.A. 1990. Changes in paleocurrents during the development of an obliquely convergent plate boundary (Sulaiman fold-belt, southwestern Himalayas, west–central Pakistan). *Sedimentary Geology*, **67**, 237–261.

Warwick, P.D., Johnson, E.A. & Khan, I.H. 1998. Collision-induced tectonism along the northwestern margin of the Indian subcontinent as recorded in the Upper Paleocene to Middle Eocene strata of central Pakistan (Kirthar and Sulaiman Ranges). *Palaeogeography, Palaeoclimatology, Palaeoecology*, **142**, 201–216.

Welcomme, J.-L. & Ginsburg, L. 1997. The evidence of an Oligocene presence in the Bugti area (Balouchistan, Pakistan). *Comptes Rendus de l'Académie des Sciences, Series IIA, Earth and Planetary Science*, **325**, 999–1004.

Welcomme, J.-L., Benammi, M., Crochet, J.-Y., Marivaux, L., Métais, G., Antoine, P.-O. & Baloch, I. S. 2001. Himalayan Forelands: palaeontological evidence for Oligocene detrital deposits in the Bugti Hills (Balochistan, Pakistan). *Geological Magazine*, **138**, 397–405.

White, N.M., Pringle, M., Garzanti, E., Bickle, M., Najman, Y., Chapman, H. & Friend, P. 2002. Constraints on the exhumation and erosion of the High Himalayan Slab, NW India, from foreland basin deposits. *Earth and Planetary Science Letters*, **195**, 29–44.

Williams, M.D. 1959. Stratigraphy of the lower Indus basin, West Pakistan. *In: Proceedings of the 5th World Petroleum Congress, New York, Section 1*. John Wiley & Sons, Chichester, 377–394.

Wu, F.-Y., Clift, P.D. & Yang, J.-H. 2007. Zircon Hf isotopic constraints on the sources of the Indus Molasse, Ladakh Himalaya, India. *Tectonics*, **26**, paper number TC2014.

Received 10 June 2010; revised typescript accepted 16 September 2010.
Scientific editing by Andrew Carter.